



# Preparation of Ag-doped g-C<sub>3</sub>N<sub>4</sub> Nano Sheet Decorated Magnetic $\gamma$ -Fe<sub>2</sub>O<sub>3</sub>@SiO<sub>2</sub> Core-Shell Hollow Spheres through a Novel Hydrothermal Procedure: Investigation of the Catalytic activity for A<sup>3</sup>, KA<sup>2</sup> Coupling Reactions and [3 + 2] Cycloaddition

Samahe Sadjadi<sup>1</sup> | Masoumeh Malmir<sup>2</sup> | Majid M. Heravi<sup>2</sup>

<sup>1</sup>Gas Conversion Department, Faculty of Petrochemicals, Iran Polymer and Petrochemical Institute, PO Box 14975-112, Tehran, Iran

<sup>2</sup>Department of Chemistry, School of Science, Alzahra University, PO Box 1993891176, Vanak, Tehran, Iran

## Correspondence

Majid Heravi, Department of Chemistry, School of Science, Alzahra University, PO Box 1993891176, Vanak, Tehran, Iran.  
Email: mmh1331@yahoo.com;  
m.heravi@alzahra.ac.ir

Samahe Sadjadi, Gas Conversion Department, Faculty of Petrochemicals, Iran Polymer and Petrochemical Institute, PO Box 14975-112, Tehran, Iran.  
Email: s.sadjadi@ippi.ac.ir;  
samahesadjadi@yahoo.com

Taking advantage of both g-C<sub>3</sub>N<sub>4</sub> and magnetic core-shell hollow spheres, for the first time a heterogeneous and magnetically separable hybrid system was prepared through a novel and simple hydrothermal procedure and used for immobilization of bio-synthesized Ag(0) nanoparticles. The hybrid system was fully characterized by using SEM/EDS, FTIR, VSM, TEM, XRD, TGA, DTGA, ICP-AES, BET and elemental mapping analysis. The catalytic utility of the obtained system, h-Fe<sub>2</sub>O<sub>3</sub>@SiO<sub>2</sub>/g-C<sub>3</sub>N<sub>4</sub>/Ag, for promoting ultrasonic-assisted A<sup>3</sup>, KA<sup>2</sup> coupling reactions and [3 + 2] cycloaddition has been confirmed. The results established that the catalyst could efficiently catalyze the reaction to afford the corresponding products in high yields in short reaction times. The reusability study confirmed that the catalyst could be recovered and reused for at least five reaction runs with only slight loss of the catalytic activity. The hot filtration test also proved low silver leaching, indicating the heterogeneous nature of the catalysis.

## KEYWORDS

[3 + 2] cycloaddition, A<sup>3</sup> and KA<sup>2</sup> coupling, g-C<sub>3</sub>N<sub>4</sub>, magnetic nanoparticles

## 1 | INTRODUCTION

In the last decade, graphitic carbon nitride (g-C<sub>3</sub>N<sub>4</sub>) as a novel form of metal-free polymeric semiconductor material has attracted great attention due to its exceptional electronic, morphological, and optical and (photo) catalytic activities.<sup>[1–4]</sup> Meanwhile, bulk g-C<sub>3</sub>N<sub>4</sub> can be facily prepared *via* poly condensation reaction of organic available precursors, such as, cyanamide,<sup>[5]</sup> dicyandiamide,<sup>[6]</sup> melamine,<sup>[7]</sup> urea, thiourea<sup>[8]</sup> etc. Generally, g-C<sub>3</sub>N<sub>4</sub> has a robust structure because of the creation of strong covalent bonds between nitrogen and carbon atoms, which is

responsible for multifunctional catalytic activity. Recently, Ong and his co-workers reviewed the significance of the graphitic carbon nitride (g-C<sub>3</sub>N<sub>4</sub>)-based photo catalysts for artificial photosynthesis and environmental remediation.<sup>[9]</sup> On the other hand, the recent researches have shown that g-C<sub>3</sub>N<sub>4</sub> is a unique support for metal nanocatalysts with high thermal and chemical stability and excellent catalytic performance in organic reactions.<sup>[10–13]</sup> Unfortunately, these materials suffered from some drawbacks such as, poor harvesting of the visible-light irradiation, low surface area, inherent low electrical conductivity and difficult recycling from the treated

solutions. Many efforts have been devoted to circumvent these issues mostly through hybridization of g-C<sub>3</sub>N<sub>4</sub> with inorganic materials.<sup>[10,11,14,15]</sup>

The utility of magnetic nanoparticles (MNPs) as cost-effective and easily separable catalysts has been proved.<sup>[16]</sup> Among various types of MNPs, hollow magnetic nanoparticles consisting of an iron oxide core with unique hollow structure have achieved more attention because of their exclusive separable features, low density, easy recovery, high surface area, self-supporting capacity and surface permeability.<sup>[17]</sup> Nano magnetic  $\gamma$ -Fe<sub>2</sub>O<sub>3</sub> hollow sphere particles have wide range of applications such as drug delivery and catalysis. Silver as an efficient catalyst has been extensively employed as a heterogeneous catalysts for promoting a range of chemical reactions including coupling reactions such as cycloadditions, cycloisomerizations, sigmatropic rearrangements, and nitrene transfer reactions.<sup>[18]</sup>

Three-component reactions of amines, alkynes and ketones or aldehydes are referred to KA<sup>2</sup> and A<sup>3</sup> coupling reactions respectively. The importance of these reactions lies in the fact that they can be applied for the synthesis of important key intermediates, propargylamines, which can be used for the synthesis of diverse range of compounds such as natural products, complex nitrogen containing chemicals with biological activities such as fungicides and herbicides and heterocycles such as pyrroles, quinolines and indolizines.<sup>[19–23]</sup> Notably, due to the advantageous of KA<sup>2</sup> and A<sup>3</sup> coupling reactions, they have been considered as potent alternative for classic methodologies for the synthesis of propargylamines such as propargylictriflates, direct amination of propargyl halides and propargylic phosphates.<sup>[21,24,25]</sup> These coupling reactions proceed in the presence of a catalyst such as gold, zinc, copper, silver, iron-based catalysts.<sup>[21,26–28]</sup> Recently, development of novel and efficient catalysts for promoting KA<sup>2</sup> and A<sup>3</sup> coupling reactions received growing attention and various catalysts including magnetic catalysts such as Fe<sub>3</sub>O<sub>4</sub>@Au nanoparticles,<sup>[29]</sup> magnetically separable CuO nanoparticles supported on graphene oxide,<sup>[30]</sup> Cu<sub>2</sub>O/nano-CuFe<sub>2</sub>O<sub>4</sub><sup>[31]</sup> and hybrid catalysts such as Cu(II) Schiff base complex immobilized on graphene oxide,<sup>[32]</sup> sulfonate-based Cu(I) metal-organic frameworks,<sup>[33]</sup> copper nanoparticles supported on starch micro particles,<sup>[34]</sup> have been reported.<sup>[35]</sup> Similarly, tetrazoles are one of the most significant intermediates used for the synthesis of more complicated compounds. They can be prepared by [3 + 2] cycloaddition reaction starting from nitriles. Generally, diverse synthetic methods have been considered for this conversion.<sup>[36–43]</sup> Despite significant advances in this research field, development of a novel efficient, non-toxic heterogeneous catalyst which could promote these reactions under green

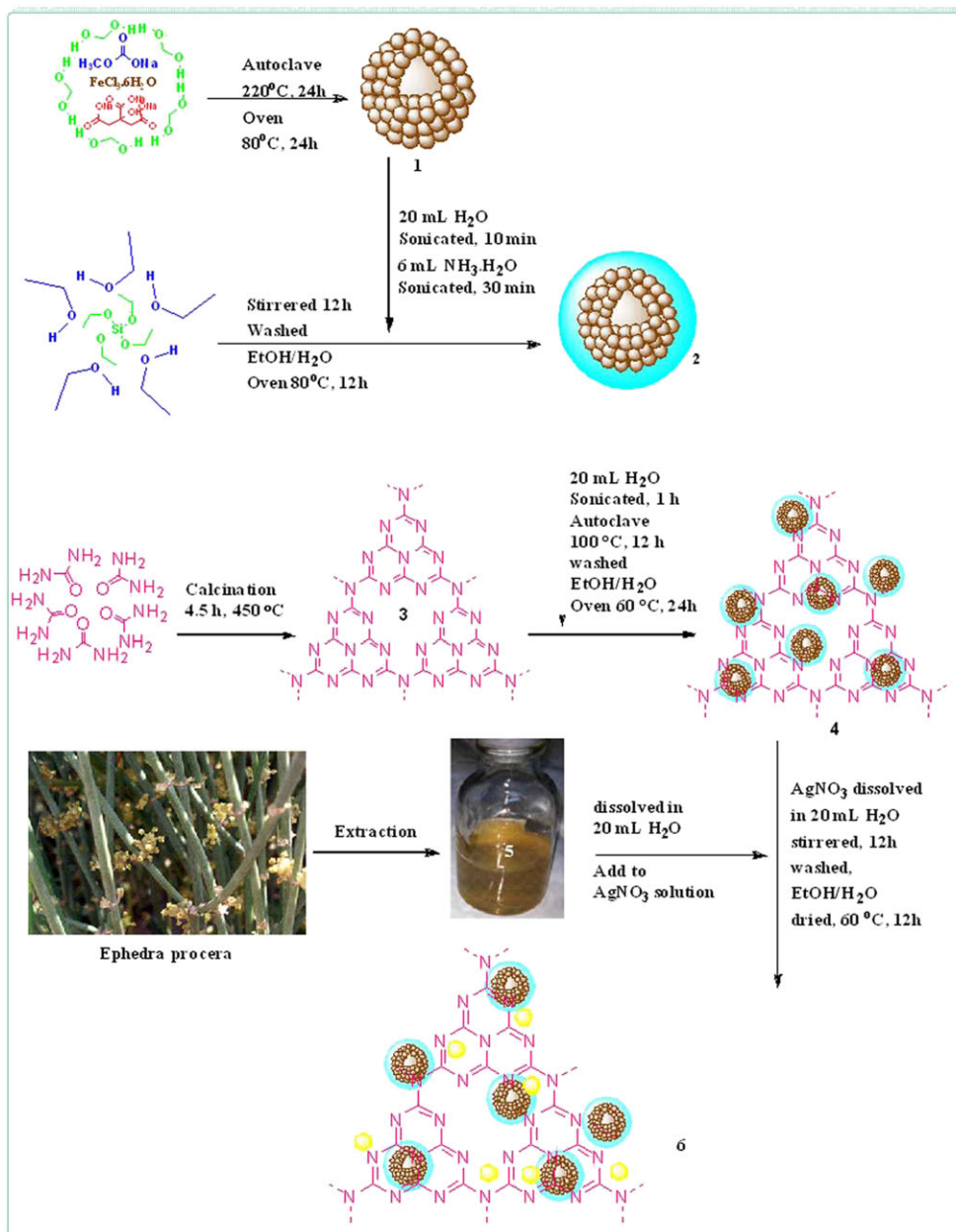
condition is still remained a hot topic. In continuation of our research on the design and preparation of heterogeneous catalysts<sup>[44,45]</sup> and development of environmentally benign procedures for the synthesis of chemicals,<sup>[44,46–49]</sup> recently, we focused on the utility of magnetic hollow spheres for developing hybrid magnetically separable heterogeneous catalysts.<sup>[35,50,51]</sup> In this line, we developed efficient catalysts by decorating magnetic hollow spheres with organic functionalities such as dopamine and cyclodextrin and doping silver nanoparticles.<sup>[50,51]</sup> Furthermore, we disclosed the use of bio-based approach for reduction of silver nanoparticles.<sup>[35,51]</sup> In all designed catalysts, the synergistic effects among the magnetic hollow spheres, organic moiety and silver nanoparticles were observed and led to promising catalysts with high catalytic activities and reusability. To further explore the hybrid catalysts based on magnetic hollow spheres, herein we wish to report for the first time, hybridization of silica-core-shell magnetic hollow spheres with g-C<sub>3</sub>N<sub>4</sub> through a novel hydrothermally-assisted procedure to develop a support for immobilization of Ag(0) nanoparticles derived from bio-based approach (Scheme 1). The catalytic activity and reusability of h-Fe<sub>2</sub>O<sub>3</sub>@SiO<sub>2</sub>/g-C<sub>3</sub>N<sub>4</sub>/Ag for promoting ultrasonic-assisted A<sup>3</sup>, KA<sup>2</sup> coupling reactions and [3 + 2] cycloaddition was also investigated.

## 2 | EXPERIMENTAL SECTION

### 2.1 | General remarks

All chemicals and reagents including, trisodium citrate dihydrate, sodium acetate trihydrate, FeCl<sub>3</sub>·6H<sub>2</sub>O, TEOS, urea, toluene, acetone, ethanol, deionized water, chloroform, dimethylformamide (DMF), ethylene glycol (EG), AgNO<sub>3</sub>, NH<sub>3</sub>·H<sub>2</sub>O, derivatives of aromatic and aliphatic aldehydes, aliphatic ketones, phenylacetylenes, benzonitriles and sodium azide in high purity were purchased from Merck and Sigma-Aldrich and used as received without further purification.

The progress of the organic reaction were monitored by TLC on commercial aluminum-backed plates of silica gel 60 F254, visualized, using ultraviolet light. Melting points were determined in open capillaries using an Electrothermal 9100 without further corrections. <sup>1</sup>H NMR and <sup>13</sup>C NMR spectra were detailed using a Bruker DRX-400 spectrometer at 400, 300 and 100, 75 MHz respectively. The h-Fe<sub>2</sub>O<sub>3</sub>@SiO<sub>2</sub>/g-C<sub>3</sub>N<sub>4</sub>/Ag was characterized by various analytical techniques including, Fourier transform infrared (FT-IR) spectroscopy, X-ray diffraction (XRD), transmission electron microscopy (TEM), field-emission scanning electron microscopy combined with electron dispersive spectrometry (FE-SEM-EDS), thermogravimetric analysis (TGA, DTGA), N<sub>2</sub>



**SCHEME 1** The possible route to the synthesis of h-Fe<sub>2</sub>O<sub>3</sub>@SiO<sub>2</sub>/g-C<sub>3</sub>N<sub>4</sub>/Ag hollow spheres

adsorption–desorption, Inductively coupled plasma atomic emission spectroscopy (ICP-AES) and vibrating sample magnetometry (VSM) were used to identify and characterize the prepared catalyst.

FTIR spectra of the fresh and reused h-Fe<sub>2</sub>O<sub>3</sub>@SiO<sub>2</sub>/g-C<sub>3</sub>N<sub>4</sub>/Ag were obtained from potassium bromide pellets in the range of 400–4000 cm<sup>-1</sup> using PERKIN-ELMER-Spectrum 65 instrument. X-ray diffraction was detected by using a Siemens, D5000. CuK $\alpha$  radiation from a sealed tube. Scanning electron Microscopy, electron dispersive spectrometry and scanning electron microscopy, analyses were performed using Tescanvega II XMU Digital Scanning Microscope and Tescan instrument, using Au-coated samples and acceleration voltage of 20 kV, respectively.

The magnetic properties of h-Fe<sub>2</sub>O<sub>3</sub>@SiO<sub>2</sub>/g-C<sub>3</sub>N<sub>4</sub>/Ag and h-Fe<sub>2</sub>O<sub>3</sub> were measured by using a vibrating sample magnetometer (VSM, Lakeshore 7407) at room temperature. BET surface area was recorded on a BELSORP Mini II instrument. The degassing process was performed by heating h-Fe<sub>2</sub>O<sub>3</sub>@SiO<sub>2</sub>/g-C<sub>3</sub>N<sub>4</sub>/Ag at 423 K for 3 h. Thermo-gravimetric analyses were conducted with a METTLER TOLEDO thermo gravimetric instrument under N<sub>2</sub> atmosphere at a heating rate of 10 °C min<sup>-1</sup> from 50 to 800 °C. The ultrasonic apparatus used for in this work was Bandelin HD 3200 with output power of 150 W and tip TT13. Transmission electron microscope images were taken with a CM30300Kv field emission transmission electron microscope.

Notably, all of compounds were known and were identified by comparison of their physical properties and spectroscopic data with those of reliable compounds and were found identical. However, we compared all compounds by their melting points. Additionally,  $^1\text{H}$  and  $^{13}\text{C}$ NMR spectra of selected compounds were recorded and given as ESI.

## 2.2 | Preparation of $\text{h-Fe}_2\text{O}_3@\text{SiO}_2/\text{g-C}_3\text{N}_4/\text{Ag}$

### 2.2.1 | General procedure for the Preparation of nanomagnetic $\text{Fe}_2\text{O}_3$ hollow sphere (1)

Hollow magnetic  $\gamma\text{-Fe}_2\text{O}_3$  was prepared *via* solvothermal method.<sup>[50]</sup> Typically, 5 mmol of ferric chloride hexahydrate was dissolved in 70 ml of ethylene glycol in a flask and then, 1.5 mmol of trisodium citrate dehydrate along with 30 mmol of sodium acetate and 17 mmol of urea was added to the solution under vigorous stirring. After 0.5 h, the as-prepared mixture was transferred into the Teflon-lined stainless-steel autoclave (150 ml capacity) and kept at 220 °C overnight. Upon completion of the hydrothermal process, the autoclave was cooled and then the precipitate was separated by an external magnet, washed with EtOH/ $\text{H}_2\text{O}$  repeatedly, and dried at 80 °C overnight in oven to obtain the brown product 1.

### 2.2.2 | General procedure for the Preparation of $\text{h-Fe}_2\text{O}_3@\text{SiO}_2$ Core shell (2)

The silica shell was formed around the  $\text{h-Fe}_2\text{O}_3$  according to the procedure reported in the literature with slight modification.<sup>[52]</sup> Typically,  $\text{h-Fe}_2\text{O}_3$  (1 g) was suspended in a mixture of ethanol (50 ml), deionized water (20 ml) and  $\text{NH}_3\cdot\text{H}_2\text{O}$  (6 ml) and then sonicated at ambient temperature by keeping the pH value at ca. 11. After 0.5 h, TEOS (2 g) was introduced into the mixture under continuous stirring at room temperature in air. After 12 h, the as-prepared 2 was collected by using an external magnet, washed several times with EtOH/ $\text{H}_2\text{O}$  to remove unreacted silica, and dried at 80 °C for 12 h in oven.

### 2.2.3 | General procedure for the synthesis of $\text{g-C}_3\text{N}_4$ Nano-sheet (3)

The  $\text{g-C}_3\text{N}_4$  nano-sheet was prepared using urea pyrolysis as described in the literature with little modification.<sup>[53]</sup> In detail, 10 g of urea was grounded into powder and then calcined at 500 °C for 4 h at a heating rate of 5 °C  $\text{min}^{-1}$ . After cooling of the crucible to room temperature, the

resulting light yellow product 3 was obtained and used in subsequent studies.

### 2.2.4 | Synthesis of $\text{h-Fe}_2\text{O}_3@\text{SiO}_2/\text{g-C}_3\text{N}_4$ (4)

In order to synthesize  $\text{h-Fe}_2\text{O}_3@\text{SiO}_2/\text{g-C}_3\text{N}_4$  core-shell, 750 mg of  $\text{h-Fe}_2\text{O}_3@\text{SiO}_2$  and 150 mg of  $\text{g-C}_3\text{N}_4$  were mixed together in deionized water (50 ml) and dispersed under ultrasonic irradiation. After 1 h, the mixture transferred to 100 ml autoclave and heated at 100 °C for 12 h. Subsequently, the brown product 4 was magnetically collected, washed for several times with EtOH/ $\text{H}_2\text{O}$  and dried in oven at 60 °C overnight.

### 2.2.5 | Preparation of Ephedra procera plant extracts (5)

Fresh leaves of Ephedra procera plant were collected around Arak City, Iran. In the first step, the collected Ephedra procera plant (5 g) was washed with deionized water, crushed in porcelain mortar to achieve soft powder. After that, it was mixed thoroughly with 100 ml deionized water and boiled at 80 °C during 1 h. After simple filtration, the fresh extract 5 was collected and used for more experiments on reduction of silver nitrate to obtain Ag (0) nanoparticles.

### 2.2.6 | Loading of Ag(0) nanoparticles on $\text{h-Fe}_2\text{O}_3@\text{SiO}_2/\text{g-C}_3\text{N}_4$ : synthesis of $\text{h-Fe}_2\text{O}_3@\text{SiO}_2/\text{g-C}_3\text{N}_4/\text{Ag}$ (6)

The immobilization and trapping of silver nanoparticles onto the surface of  $\text{h-Fe}_2\text{O}_3@\text{SiO}_2/\text{g-C}_3\text{N}_4$  was performed by a novel, bio-based and green procedure. In this line, to the stirring mixture of  $\text{h-Fe}_2\text{O}_3@\text{SiO}_2/\text{g-C}_3\text{N}_4$  (1 g) in 20 ml deionized water, a solution of  $\text{AgNO}_3$  (0.1 g) in 20 ml deionized water was added at room temperature. After 0.5 h, the  $\text{Ag}^+$  ions were adsorbed onto the surfaces of  $\text{h-Fe}_2\text{O}_3@\text{SiO}_2/\text{g-C}_3\text{N}_4$  through the electrostatic interaction. To reduce silver salt and obtain Ag(0) nanoparticles, Ephedra procera was used as a reducing and stabilizing agent. To this purpose, the fresh extract (1 ml) was added into the stirred suspension for 12 h. Upon completion of the process; the black product 6 was magnetically collected, washed three times with EtOH/ $\text{H}_2\text{O}$  and dried at 60 °C for 12 h.

All steps of the procedure led to the formation of nanomagnetic  $\text{h-Fe}_2\text{O}_3@\text{SiO}_2/\text{g-C}_3\text{N}_4/\text{Ag}$  as a catalyst are illustrated in Scheme 1.

## 2.2.7 | General procedure for the synthesis of propargylamine (A<sup>3</sup> Coupling reaction): (5 l)

The amount of 20 mg of h-Fe<sub>2</sub>O<sub>3</sub>@SiO<sub>2</sub>/g-C<sub>3</sub>N<sub>4</sub>/Ag as a catalyst was added to a mixture of phenyl acetylene (1.1 mmol), aldehyde (1.0 mmol) and amine (1.0 mmol) in 10 ml H<sub>2</sub>O as a green solvent. The resulting mixture was then subjected to ultrasonic radiation of 80 W for suitable reaction time (monitored by TLC). After completion of the reaction, the mixture was cooled to room temperature and diluted with hot ethanol (10 ml). The catalyst was magnetically separated, washed with ethanol, dried in air and re-used for a consecutive run. The resulting product was purified by recrystallization (hot ethanol) to obtain the excellent yield.

## 2.2.8 | General procedure for the synthesis of 1H-tetrazoles ([3 + 2] Cycloaddition): (9a)

The amount of 30 mg of h-Fe<sub>2</sub>O<sub>3</sub>@SiO<sub>2</sub>/g-C<sub>3</sub>N<sub>4</sub>/Ag was added to a mixture of nitrile (1.0 mmol) and NaN<sub>3</sub> (1.5 mmol) in DMF (5 ml). The mixture was sonicated with power of 100 W for appropriate reaction time until the reaction was completed (monitored by TLC). After completion of reaction, the mixture was cooled to room temperature and diluted with ethyl acetate (10 ml) and 5 N HCl (20 ml). The catalyst was magnetically separated by using an external magnet, washed with ethanol, dried in oven and re-used for a consecutive run. Furthermore, the organic layer was separated, and the aqueous layer was extracted with ethyl acetate (20 ml). The combined ethyl acetate layer was washed with water, dried over anhydrous Na<sub>2</sub>SO<sub>4</sub>. The residue was purified by recrystallization and short column chromatography on silica gel to obtain the main products.

## 3 | RESULTS AND DISCUSSION

### 3.1 | Characterization of the catalyst

#### 3.1.1 | FT-IR Spectra

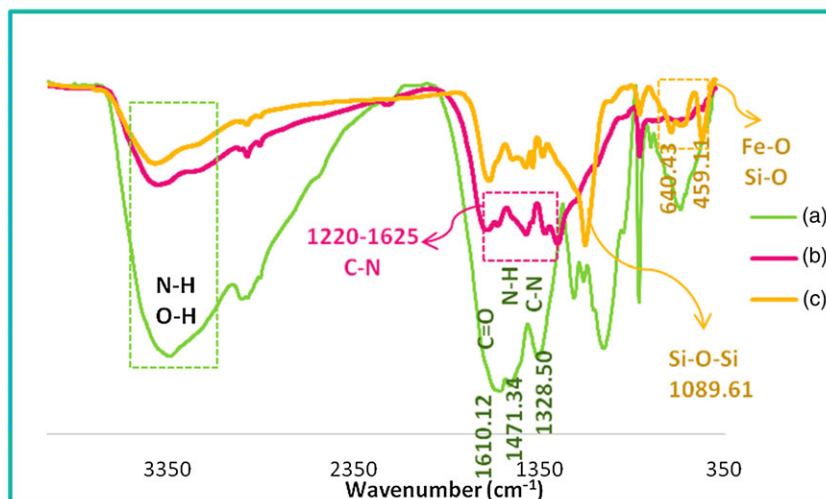
The FTIR spectroscopy was used to confirm the formation of g-C<sub>3</sub>N<sub>4</sub> and h-Fe<sub>2</sub>O<sub>3</sub>@SiO<sub>2</sub>/g-C<sub>3</sub>N<sub>4</sub>/Ag, Figure 1. The FTIR spectrum of g-C<sub>3</sub>N<sub>4</sub> exhibited a characteristic band at 3000–3500 cm<sup>-1</sup> which is representative of N-H and O-H groups. Moreover, the observed band at 1200–1600 cm<sup>-1</sup> is indicative of C-N group. This spectrum is in good accordance with the previous reports in the literature.<sup>[54]</sup> To further confirm the formation of g-C<sub>3</sub>N<sub>4</sub>, the spectra of pure urea and g-C<sub>3</sub>N<sub>4</sub> were compared, Figure 1. As depicted, the two FTIR spectra are markedly distinguished. Urea exhibited a sharp band at 1610 cm<sup>-1</sup> which is representative of C=O group. The absence of this band in the FTIR spectrum of g-C<sub>3</sub>N<sub>4</sub> can prove its successful formation.

The FTIR spectrum of the h-Fe<sub>2</sub>O<sub>3</sub>@SiO<sub>2</sub>/g-C<sub>3</sub>N<sub>4</sub>/Ag, Figure 1, showed sharp absorption bands at 470–590 cm<sup>-1</sup> which can be related to Fe-O stretching vibration, indicating the formation of magnetic NPs.<sup>[50]</sup> Furthermore, the characteristic band at 1089 cm<sup>-1</sup> is representative of Si-O stretching and can confirm the presence of silica shell. The absorption bands at 976, 825 and 475 cm<sup>-1</sup> can be attributed to the bending vibrations of the Si-O-Si bond.<sup>[55]</sup> The bands at range of 1225–1645 cm<sup>-1</sup>, which are the characteristic bands of g-C<sub>3</sub>N<sub>4</sub> are present in both spectra of h-Fe<sub>2</sub>O<sub>3</sub>@SiO<sub>2</sub>/g-C<sub>3</sub>N<sub>4</sub>/Ag and g-C<sub>3</sub>N<sub>4</sub> and can indicate the conjugation of g-C<sub>3</sub>N<sub>4</sub>.

#### 3.1.2 | SEM-EDS images

Initially, the formation of g-C<sub>3</sub>N<sub>4</sub> was confirmed by SEM-EDS analyses, Figure 2. The observed morphology

**FIGURE 1** The FTIR spectra of a) pure urea, b) pure g-C<sub>3</sub>N<sub>4</sub> and c) h-Fe<sub>2</sub>O<sub>3</sub>@SiO<sub>2</sub>/g-C<sub>3</sub>N<sub>4</sub>/Ag



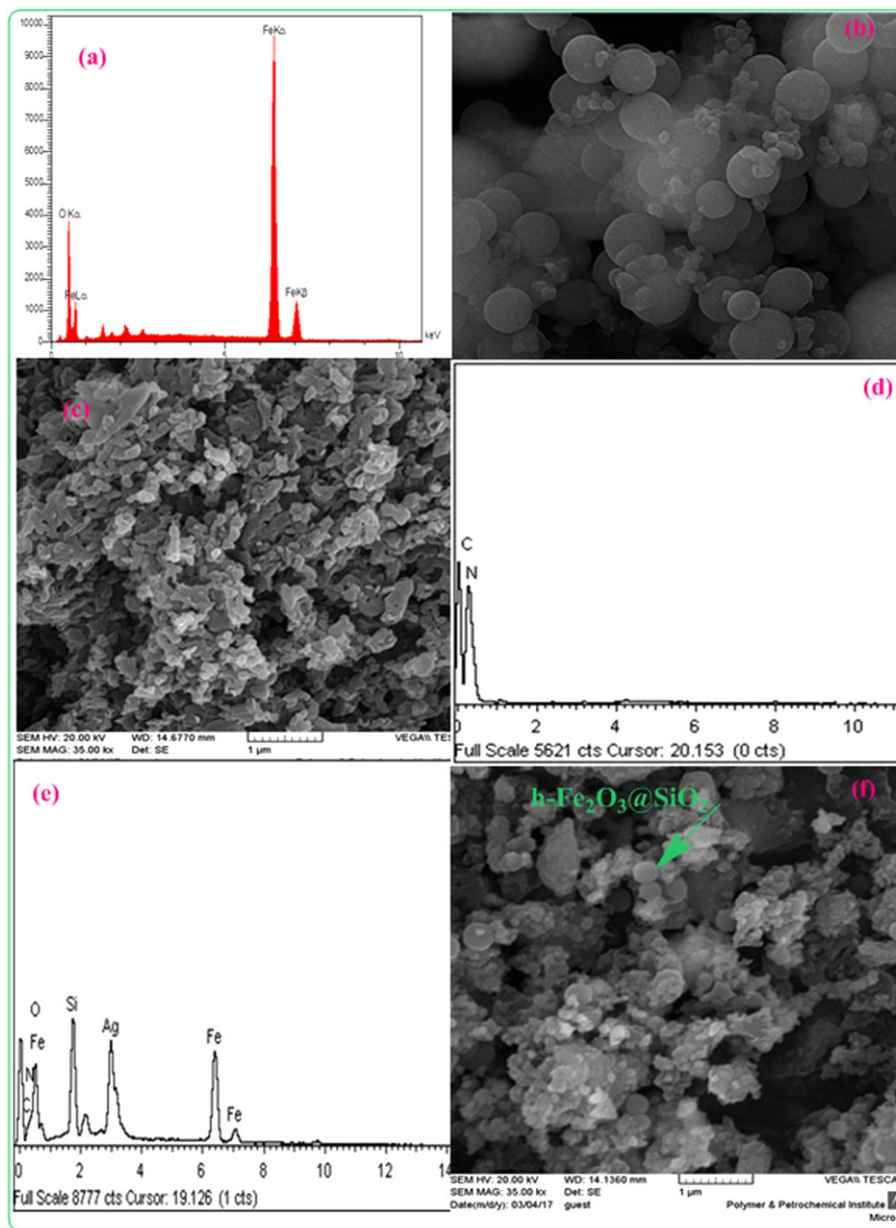


**FIGURE 2** The FE-SEM-EDS analysis of a,b)  $\text{h-Fe}_2\text{O}_3$ , the SEM-EDS analysis of b,c) pure  $\text{g-C}_3\text{N}_4$  and e,f)  $\text{h-Fe}_2\text{O}_3@/\text{SiO}_2/\text{g-C}_3\text{N}_4/\text{Ag}$

of  $\text{g-C}_3\text{N}_4$  is in good agreement with previous reports.<sup>[56]</sup> The EDS analysis also contains only C and N atoms, indicating the formation of  $\text{g-C}_3\text{N}_4$ . To study the morphology of  $\text{h-Fe}_2\text{O}_3@/\text{SiO}_2/\text{g-C}_3\text{N}_4/\text{Ag}$  and elucidate whether the formation of silica shell and incorporation of  $\text{g-C}_3\text{N}_4$  and Ag nanoparticle could alter the morphology, the FE-SEM-EDS images of  $\text{h-Fe}_2\text{O}_3$  as well as SEM-EDS images of the  $\text{h-Fe}_2\text{O}_3@/\text{SiO}_2/\text{g-C}_3\text{N}_4/\text{Ag}$  were recorded and compared, Figure 2. As expected,<sup>[50]</sup>  $\text{h-Fe}_2\text{O}_3$  possessed the spherical morphology (Figure 2b). The  $\text{h-Fe}_2\text{O}_3@/\text{SiO}_2/\text{g-C}_3\text{N}_4/\text{Ag}$  also showed a spherical morphology, however, its morphology was more aggregated. Considering the morphology of  $\text{g-C}_3\text{N}_4$ , it can be clearly detected that the spherical magnetic

nanoparticles are surrounded with  $\text{g-C}_3\text{N}_4$ . This observation can confirm that the spherical morphology of magnetic nanoparticles did not change upon decoration with  $\text{g-C}_3\text{N}_4$  and Ag nanoparticle. However, the presence of  $\text{g-C}_3\text{N}_4$  on the surface of the nanoparticles kept them more closed and packed.

The EDS image of  $\text{h-Fe}_2\text{O}_3@/\text{SiO}_2/\text{g-C}_3\text{N}_4/\text{Ag}$  clearly shows the presence of Fe and O atoms which can be representative of magnetic nanoparticles (Figure 2e). The presence of Si and O atoms can also confirm the formation of silica shell. Moreover, the observation of C and N in EDS can be indicative of  $\text{g-C}_3\text{N}_4$ . Finally, the incorporation of silver nanoparticles can be confirmed by observing Ag atom in EDS.

### 3.1.3 | Elemental mapping analysis

In Figure 3, the elemental mapping analysis of h-Fe<sub>2</sub>O<sub>3</sub>@SiO<sub>2</sub>/g-C<sub>3</sub>N<sub>4</sub>/Ag is depicted. As shown, the dispersions of C and N atoms are almost uniform, indicating that g-C<sub>3</sub>N<sub>4</sub> has successfully covered the magnetic core-shell h-Fe<sub>2</sub>O<sub>3</sub>@SiO<sub>2</sub>. Additionally, Ag atoms are also well-dispersed on the surface of the catalyst and no aggregation is detected. This observation can confirm the efficiency of g-C<sub>3</sub>N<sub>4</sub> for having electrostatic interactions with silver nanoparticles and preventing them from aggregation.

### 3.1.4 | XRD analysis

The formation of desired phases in h-Fe<sub>2</sub>O<sub>3</sub>@SiO<sub>2</sub>/g-C<sub>3</sub>N<sub>4</sub>/Ag was confirmed by obtaining X-ray diffraction pattern, XRD, Figure 4. The observed peaks at  $2\theta = 30.0, 35.5, 43.2, 54.7, 57.1, 63.8$  and  $74.0^\circ$  (labeled

as F) were in good agreement with the {220}, {311}, {400}, {422}, {511}, {440} and {533} planes of the typical cubic structure hematite (JCPDS card no. 39-1346)<sup>[50]</sup> and confirm the formation of magnetic nanoparticles. The peaks at  $2\theta = 38.0, 44.1, 64.3, 77.8, 81.0^\circ$  (labeled as A) are indicative of formation of Ag(0) nanoparticles (JCPDS card no. 04-0783). It is worth noting that the broad halo present at  $2\theta = 5.0-27.0^\circ$  (labeled as \*) can be assigned to the amorphous silica and g-C<sub>3</sub>N<sub>4</sub>.

### 3.1.5 | Vibrating sample magnetometer (VSM) analysis

Next, the magnetic properties of h-Fe<sub>2</sub>O<sub>3</sub>@SiO<sub>2</sub>/g-C<sub>3</sub>N<sub>4</sub>/Ag was studied by room temperature vibrating sample magnetometer (VSM) and compared with that of h-Fe<sub>2</sub>O<sub>3</sub>, Figure 5. Interestingly, the results established that incorporation of nanomagnetic SiO<sub>2</sub> shell, g-C<sub>3</sub>N<sub>4</sub> and

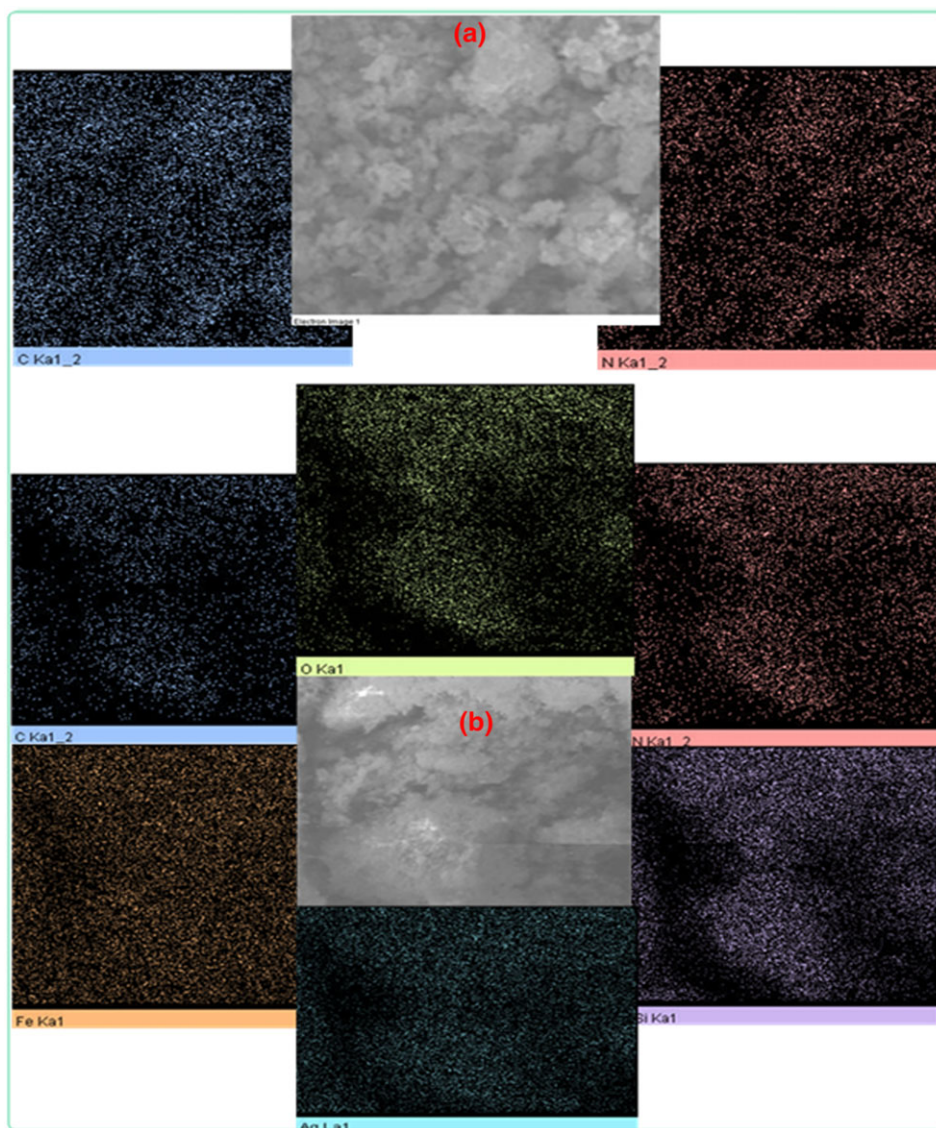


**FIGURE 3** The Map analysis of a) pure g-C<sub>3</sub>N<sub>4</sub> and b) h-Fe<sub>2</sub>O<sub>3</sub>@SiO<sub>2</sub>/g-C<sub>3</sub>N<sub>4</sub>/Ag

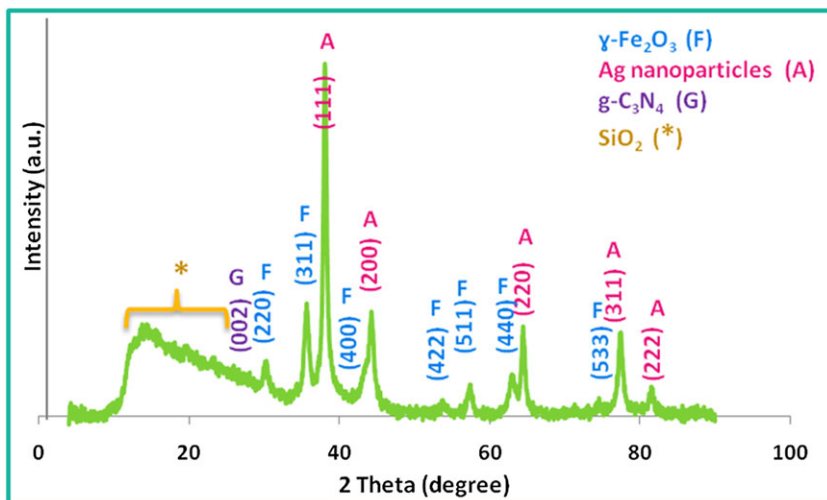


**FIGURE 4** XRD analysis of h-Fe<sub>2</sub>O<sub>3</sub>@SiO<sub>2</sub>/g-C<sub>3</sub>N<sub>4</sub>/Ag

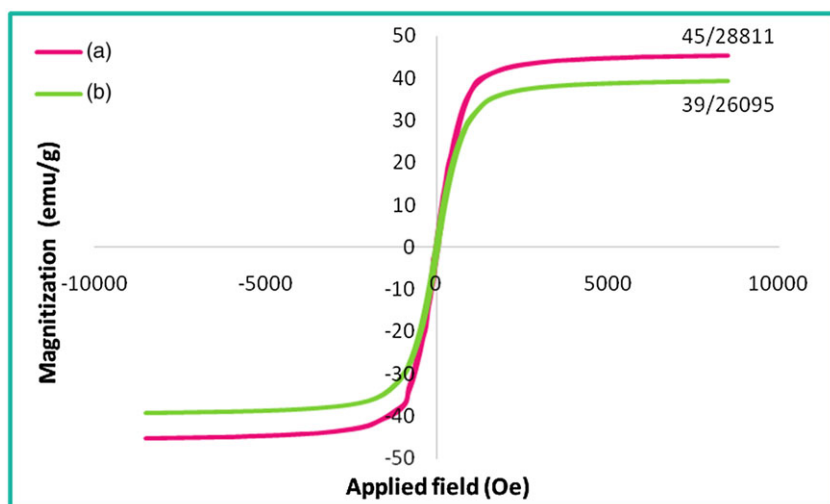


**FIGURE 5** VSM analyses of the a) h-Fe<sub>2</sub>O<sub>3</sub> and b) h-Fe<sub>2</sub>O<sub>3</sub>@SiO<sub>2</sub>/g-C<sub>3</sub>N<sub>4</sub>/Ag

Ag(0) nanoparticles only led to a slight decrease in the maximum saturation magnetization ( $M_s$ ) values of h-Fe<sub>2</sub>O<sub>3</sub> (from 45.25 emu g<sup>-1</sup> to 39.26 emu g<sup>-1</sup>) and the hysteresis loops of h-Fe<sub>2</sub>O<sub>3</sub>@SiO<sub>2</sub>/g-C<sub>3</sub>N<sub>4</sub>/Ag exhibited a super paramagnetic behavior and could be separated simply by using an external magnet. This finding can be considered very important as mostly introduction of nanomagnetic components to a magnetic nanoparticle could reduce the  $M_s$  remarkably.<sup>[35]</sup> Notably, no significant change in the coercivity from the enlarged view of the central loop of the h-Fe<sub>2</sub>O<sub>3</sub> and h-Fe<sub>2</sub>O<sub>3</sub>@SiO<sub>2</sub>/g-C<sub>3</sub>N<sub>4</sub>/Ag was observed.

### 3.1.6 | Thermogravimetric analysis (TGA)

The thermal stability of the h-Fe<sub>2</sub>O<sub>3</sub>@SiO<sub>2</sub>/g-C<sub>3</sub>N<sub>4</sub>/Ag was also investigated by thermogravimetric analyses (TGA and DTGA), Figure 6. As depicted in Figure 6, the thermogram of the catalyst exhibited five degradation steps over the range of 30–800 °C. According to the literature,<sup>[50]</sup> the first

weight loss, occurred at about 200 °C, can be assigned to the loss of adsorbed H<sub>2</sub>O molecules and/ or surface hydroxyl groups. The other observed weight losses can be assigned to the degradation of organic component of h-Fe<sub>2</sub>O<sub>3</sub>@SiO<sub>2</sub>/g-C<sub>3</sub>N<sub>4</sub>/Ag. Using this analysis, the content of organic component in h-Fe<sub>2</sub>O<sub>3</sub>@SiO<sub>2</sub>/g-C<sub>3</sub>N<sub>4</sub>/Ag was calculated to be 20.622 w/w%.

Subsequently, the weight percentage of Ag in h-Fe<sub>2</sub>O<sub>3</sub>@SiO<sub>2</sub>/g-C<sub>3</sub>N<sub>4</sub>/Ag was studied by using ICP-AES analysis. To this purpose, a known amount of h-Fe<sub>2</sub>O<sub>3</sub>@SiO<sub>2</sub>/g-C<sub>3</sub>N<sub>4</sub>/Ag was digested in concentrated HNO<sub>3</sub> and HCl solution. The analysis of the obtained extract by ICP-AES showed that the Ag content was about 0.8 w/w%.

### 3.1.7 | N<sub>2</sub> adsorption–desorption

In Figure 7, the nitrogen adsorption–desorption isotherm of h-Fe<sub>2</sub>O<sub>3</sub>@SiO<sub>2</sub>/g-C<sub>3</sub>N<sub>4</sub>/Ag is depicted. The surface area of h-Fe<sub>2</sub>O<sub>3</sub>@SiO<sub>2</sub>/g-C<sub>3</sub>N<sub>4</sub>/Ag was calculated to be

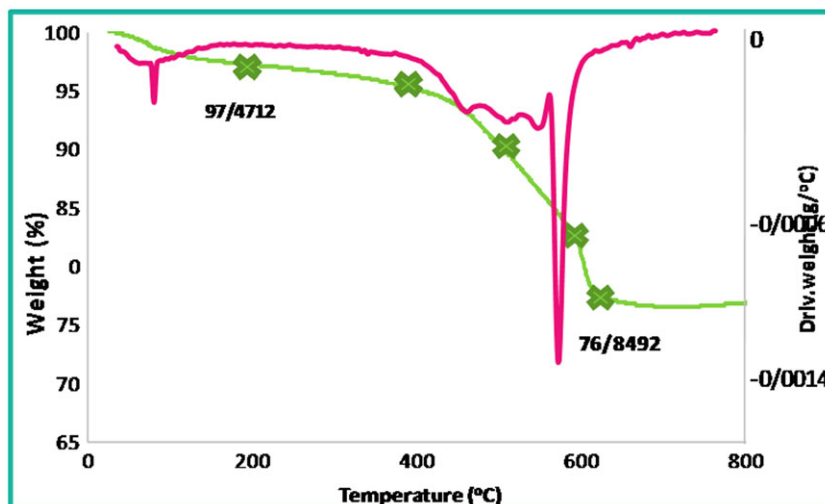


**FIGURE 6** The TGA and DTGA analyses of the h-Fe<sub>2</sub>O<sub>3</sub>@SiO<sub>2</sub>-CD/Ag

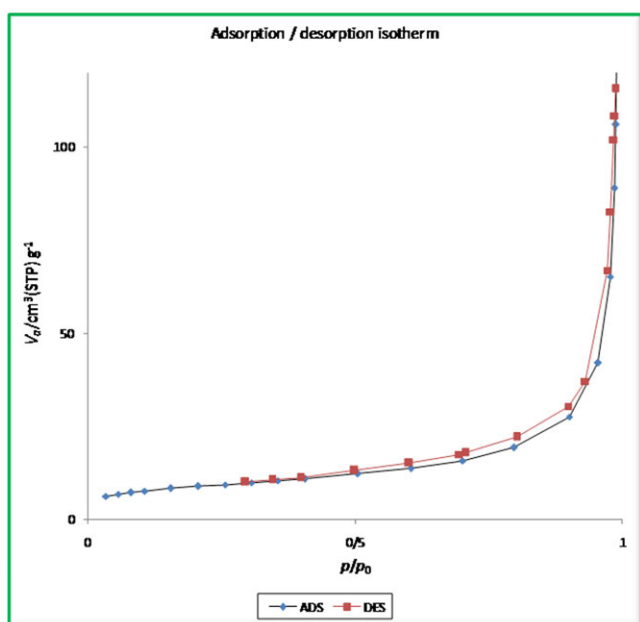


**FIGURE 7** The N<sub>2</sub> adsorption-desorption, BET and BJH isotherms of the h-Fe<sub>2</sub>O<sub>3</sub>@SiO<sub>2</sub>/g-C<sub>3</sub>N<sub>4</sub>/Ag

30 m<sup>2</sup> g<sup>-1</sup>. Moreover, the value of the total pore volume, average pore diameter and pore size of the catalyst were 0.22 cm<sup>3</sup> g<sup>-1</sup>, 29.3 and nm respectively, Table 1. It is concluded that the catalyst possesses a porous structure. Furthermore, based on to IUPAC classification the isotherm showed type IV nitrogen adsorption-desorption isotherms with H3 hysteresis loops<sup>[57]</sup> which was usually found on solids, indicating the presence of large mesopores with a broad size distribution. Regarding to

**TABLE 1** Textural property of h-Fe<sub>2</sub>O<sub>3</sub>@SiO<sub>2</sub>/g-C<sub>3</sub>N<sub>4</sub>/Ag

Catalyst	S <sub>BET</sub> (m <sup>2</sup> g <sup>-1</sup> )	Total pore volume (cm <sup>3</sup> g <sup>-1</sup> )	Average pore diameter (nm)	Pore size (nm)
h-Fe <sub>2</sub> O <sub>3</sub> @SiO <sub>2</sub> /g-C <sub>3</sub> N <sub>4</sub> /Ag	30	0.22	29.3	3.28

experimental results, isotherm of type IV confirms the presence a typical hysteresis loop of mesoporous adsorbents with a pore size diameter between 2 nm and 50 nm with a maximum around 3 nm.

### 3.1.8 | TEM analysis

h-Fe<sub>2</sub>O<sub>3</sub>@SiO<sub>2</sub>/g-C<sub>3</sub>N<sub>4</sub>/Ag was also studied by TEM, Figure 8. As shown, core-shell spheres can be observed in which the darker core is the magnetic nanoparticle while the lighter shell is silica with an average thickness of about 40 nm. Ag nanoparticles can be detected as small dark spots with an average diameter of about less than 10 nm. The formation of g-C<sub>3</sub>N<sub>4</sub> can clearly confirmed by observing the sheets on the sphere.

## 3.2 | Catalytic activity of the h-Fe<sub>2</sub>O<sub>3</sub>@SiO<sub>2</sub>/g-C<sub>3</sub>N<sub>4</sub>/Ag

### 3.2.1 | A<sup>3</sup> and KA<sup>2</sup> coupling reactions

In the next step, the catalytic activity of the h-Fe<sub>2</sub>O<sub>3</sub>@SiO<sub>2</sub>/g-C<sub>3</sub>N<sub>4</sub>/Ag was investigated. To this purpose, the three-component reaction of amines, phenyl acetylene and aldehydes or ketones, A<sup>3</sup> and KA<sup>2</sup>, which is one of the most important approaches for the synthesis of propargylamines, were selected as the model organic transformations. To develop a green, eco-friendly and rapid procedure, the use of ultrasonic irradiation was targeted. Initially, the reaction of phenyl acetylene, benzaldehyde, and morpholine was selected as a model reaction, Scheme 2. To establish the necessity of the

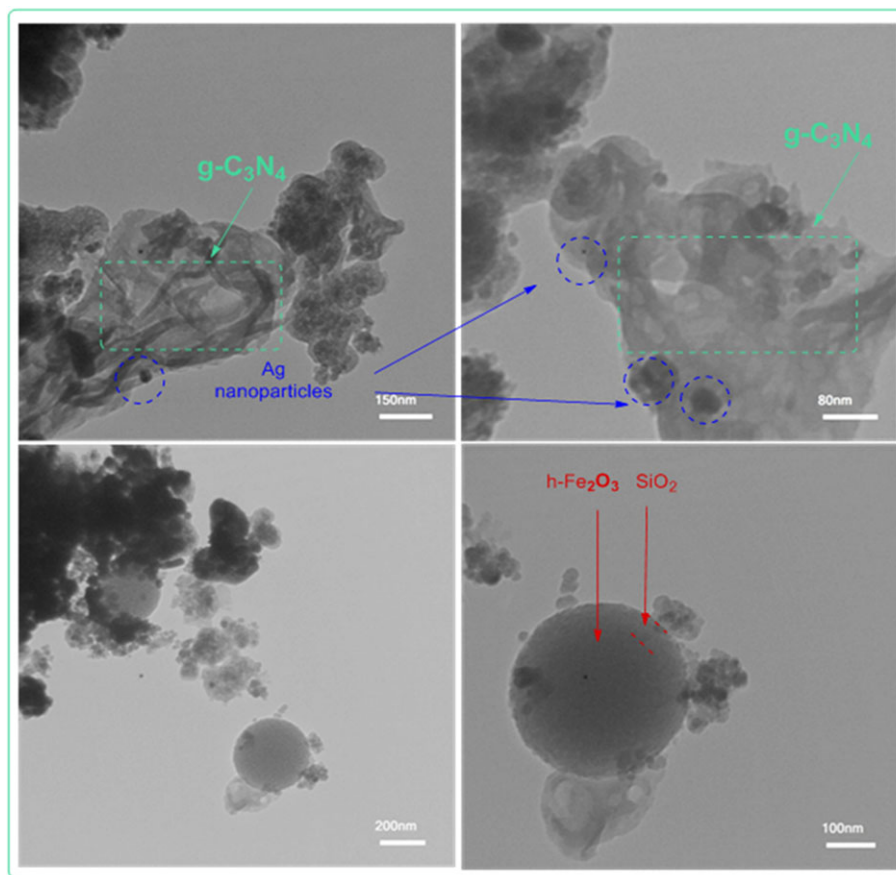
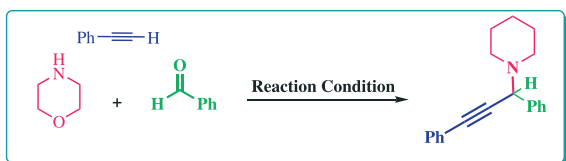


**FIGURE 8** The TEM images of  $h\text{-Fe}_2\text{O}_3@SiO_2/g\text{-C}_3\text{N}_4/Ag$



**SCHEME 2** Model reaction of propargylamine

presence of the catalyst for promoting the synthesis of propargylamines, the model reaction was performed in the absence of the catalyst. The result established that the reaction did not proceed without the catalyst. Next, the reaction variables were optimized by performing the model reaction by using different ultrasonic power (40–100 w) in the presence of various amounts of the catalyst (10–30 mg), in various solvents including (ethanol, water, chloroform, DMF) and solvent free condition, Figure 9. The results demonstrated that increasing the catalyst amount from 10 mg to 20 mg led to the increase in the yield of the model product. However, further increase of the catalyst to 30 mg had no positive effect on the yield of the desired product. Moreover, water was selected as the solvent of the choice. It was also shown that the power of ultrasonic irradiation can clearly affect the yield of the product. Increasing the power of ultrasonic

irradiation from 40 W to 80 W increased the yield of the desired product while further increase in this value had a detrimental effect and lower yields were obtained using power of 100 W. This observation can be attributed to the acceleration of the formation of some side-products upon using high ultrasonic powers. Using all these results, the optimum reaction condition was selected to be using 20 mg catalyst in water as solvent under ultrasonic power of 80 W.

Having the optimum reaction variables in hand, the generality of the protocol was studied by using various amines, aldehydes and ketones, Tables 2 and 3. As shown in Tables 2 and 3, this protocol exhibited high substrate scope and various substrates with different electron densities and steric properties can be successfully used in this protocol to lead to the corresponding products in high yields in short reaction times.

#### Plausible Reaction Mechanism

The plausible reaction mechanism for  $A^3$  and  $KA^2$  coupling reactions is depicted in Scheme 3. Based on the previous reports,<sup>[50,58]</sup> the reaction can initiate by the formation of Ag-acetylide I which can be obtained through activation of terminal C-H bond of phenylacetylene by silver nanoparticles of  $h\text{-Fe}_2\text{O}_3@SiO_2/g\text{-C}_3\text{N}_4/Ag$ .

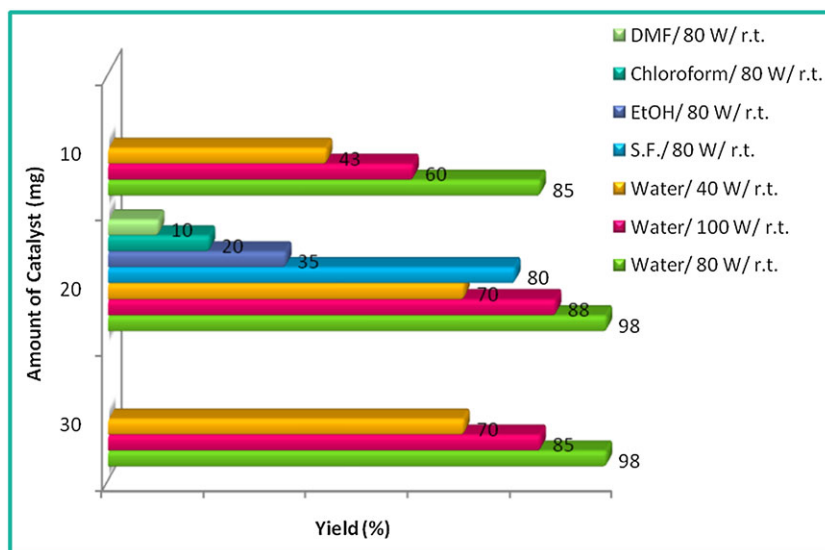


**FIGURE 9** Effects of loading of catalyst, duration of reaction and solvent for the synthesis of propargylamine

Subsequently, the formed intermediate can undergo reaction with iminium ion, II, produced from condensation reaction of aldehyde and amine to furnish  $h\text{-Fe}_2\text{O}_3\text{@SiO}_2/\text{g-C}_3\text{N}_4/\text{Ag}$  and the desired product.

### 3.2.2 | [3 + 2] cycloaddition

Motivated by high catalytic activity of  $h\text{-Fe}_2\text{O}_3\text{@SiO}_2/\text{g-C}_3\text{N}_4/\text{Ag}$ , we further investigated its performance for promoting synthesis of 5-substituted 1*H*-tetrazoles through two component reaction of nitriles and sodium azide. Similar to the propargylamine synthesis, the ultrasonic-assisted procedure was selected and the reaction condition was optimized by choosing a model reaction, the reaction of benzonitriles and sodium azide (Scheme 4), and varying the reaction variables, i.e. catalyst amount, ultrasonic power and solvent, Figure 10. As shown in Figure 10, the optimum reaction condition was using 30 mg catalyst in DMF under ultrasonic irradiation of power 100 W. Next, the generality of the protocol was confirmed by using various nitriles, Table 4. As shown, this protocol exhibited broad substrate scope and aromatic, heterocyclic and aliphatic substrates can tolerate the reaction to furnish the corresponding products. In the case of benzonitrile, the presence of electron-donating substituents on the aromatic ring led to sluggish reactions due to the reduced the electrophilic character of benzonitrile.

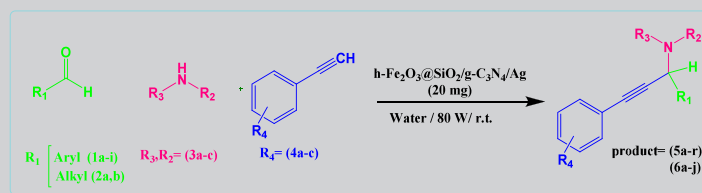
#### Plausible Reaction Mechanism

According to the previous reports,<sup>[59]</sup> the plausible mechanism for the synthesis of 1*H*-Tetrazole is initial activation of nitrile groups by silver nanoparticles of  $h\text{-Fe}_2\text{O}_3\text{@SiO}_2/\text{g-C}_3\text{N}_4/\text{Ag}$  which can serve as a Lewis acid and formation of intermediate I followed by reaction

with sodium azide and formation of intermediate II and cyclization, Scheme 5.

### 3.3 | Reusability of the catalyst

The simple recovery and reusability are requisites of heterogeneous catalysts with industrial use. Hence, investigation of the catalysts is imperative. To study the reusability of the  $h\text{-Fe}_2\text{O}_3\text{@SiO}_2/\text{g-C}_3\text{N}_4/\text{Ag}$ , the yields of two model reactions were obtained using fresh catalyst. Upon completion of the reaction, the catalyst was separated magnetically, washed and reused for successive reaction runs. The results, Figure 11, established that the catalyst exhibited high reusability and could be reused for several reaction runs with only slight loss of the catalytic activity. Comparing the reusability of the catalyst for two model reactions, demonstrated that the catalyst showed superior reusability for the synthesis of propargylamine (the catalyst could be reused for seven reaction runs) than synthesis of 1*H*-tetrazole (the catalyst preserved its catalytic activity for five reaction runs). This observation can be attributed to the use of higher ultrasonic power for the synthesis of 1*H*-tetrazole, which may induce the leaching of Ag(0) nanoparticles. To confirm this speculation, the leachings of the silver nanoparticles for both model reactions were studied *via* ICP-AES for the catalyst reused for fifth and seventh reaction runs. The results showed that up to five reuse, the leaching of silver was negligible for both reactions. However, the leaching after seventh reuse for the synthesis of 1*H*-tetrazole was much higher than that of synthesis of propargylamine. This observation not only established the dependency of reusability of the catalyst on the reaction condition, indicated that the nature of the catalysis is heterogeneous and the catalytic reaction

**TABLE 2** Synthesis of three-component reaction of derivatives aldehyde, secondary- amines and terminal alkynes catalyzed by h-Fe<sub>2</sub>O<sub>3</sub>@SiO<sub>2</sub>/g-C<sub>3</sub>N<sub>4</sub>/Ag<sup>a</sup> [50]

R <sub>1</sub>	R <sub>2</sub>	R <sub>3</sub>	R <sub>4</sub>	Product	Time (min)	Yield <sup>b</sup> (%)
1a: C <sub>6</sub> H <sub>5</sub>	3a: -(CH <sub>2</sub> ) <sub>5</sub> -		4a: C <sub>6</sub> H <sub>5</sub>	<b>5a</b>	15	95
1b: <i>p</i> -Cl-C <sub>6</sub> H <sub>4</sub>	3a		4a	<b>5b</b>	15	88
1c: <i>o</i> -Cl-C <sub>6</sub> H <sub>4</sub>	3a		4a	<b>5c</b>	20	89
1d: <i>p</i> -Br-C <sub>6</sub> H <sub>4</sub>	3a		4a	<b>5d</b>	15	92
1e: <i>p</i> -Me-C <sub>6</sub> H <sub>4</sub>	3a		4a	<b>5e</b>	20	90
1f: <i>p</i> -MeO-C <sub>6</sub> H <sub>4</sub>	3a		4a	<b>5f</b>	18	86
1 g: <i>o</i> -Thiophen	3a		4a	<b>5 g</b>	16	93
1 h: <i>p</i> -OHCC <sub>6</sub> H <sub>4</sub>	3a		4a	<b>5 h</b>	25	90
1i: <i>o</i> -Naphthyl	3a		4a	<b>5i</b>	12	94
1a	3a		4b: <i>p</i> -CH <sub>3</sub> -C <sub>6</sub> H <sub>4</sub>	<b>5j</b>	20	88
1a	3a		4c: <i>p</i> -F-C <sub>6</sub> H <sub>4</sub>	<b>5 k</b>	25	83
1a	3b(CH <sub>2</sub> ) <sub>2</sub> -O-(CH <sub>2</sub> ) <sub>2</sub> -		4a	<b>5 l</b>	12	98
1b	3b		4a	<b>5 m</b>	15	91
1e	3b		4a	<b>5n</b>	18	90
1d	3b		4a	<b>5o</b>	16	90
1a	3b		4b	<b>5p</b>	20	92
1a	3c: -(CH <sub>2</sub> ) <sub>4</sub> -		4a	<b>5q</b>	15	80
1a	3d: C <sub>2</sub> H <sub>5</sub>	C <sub>2</sub> H <sub>5</sub>	4a	<b>5r</b>	13	73
2a: C <sub>6</sub> H <sub>11</sub>	3a		4a	<b>6a</b>	15	90
2a	3b		4b	<b>6b</b>	15	83
2a	3b		4a	<b>6c</b>	18	88
2a	3c		4a	<b>6d</b>	20	90
2a	3d		4a	<b>6e</b>	25	75
2a	3a		4c	<b>6f</b>	20	85
2b: -(CH <sub>2</sub> ) <sub>2</sub> -Me	3a		4a	<b>6 g</b>	15	85
2b	3b		4a	<b>6 h</b>	18	75
2b	3c		4a	<b>6i</b>	17	79
2b	3d		4a	<b>6j</b>	20	75

<sup>a</sup>Reaction conditions: aliphatic or arylaldehydes (1 mmol), amines (1 mmol), alkynes (1.1 mmol), h-Fe<sub>2</sub>O<sub>3</sub>@SiO<sub>2</sub>/g-C<sub>3</sub>N<sub>4</sub>/Ag (20 mg) in water at 80 W and room temperature.

<sup>b</sup>Isolated yield.

did not proceed through leached silver nanoparticles. Finally, the stability of the catalyst in the course of the catalytic process was studied by comparing the FTIR

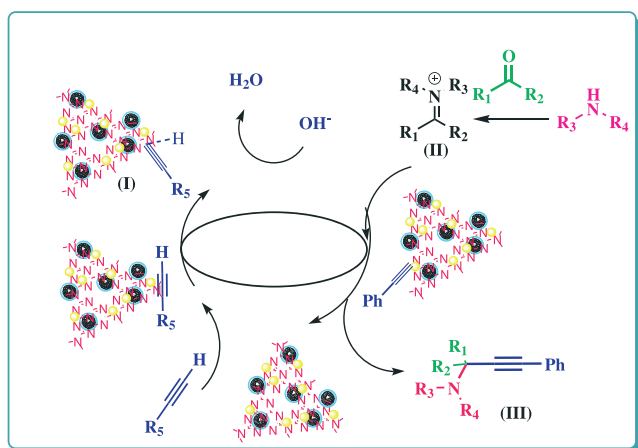
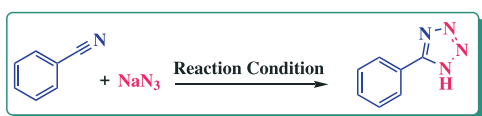
spectra of the fresh and the reused catalyst after five reaction runs, Figure 12. The results established that both FTIR spectra were almost similar, indicating that

**TABLE 3** Synthesis of the three-component reaction of aliphatic ketones, secondary- amines and terminal alkynes catalyzed by h-Fe<sub>2</sub>O<sub>3</sub>@SiO<sub>2</sub>/g-C<sub>3</sub>N<sub>4</sub>/Ag<sup>[50]</sup>


R <sub>5</sub> , R <sub>6</sub>	R <sub>3</sub> , R <sub>4</sub>	R <sub>4</sub>	Product	Time (min)	Yield <sup>b</sup> (%)
7a: -(CH <sub>2</sub> ) <sub>4</sub> -	3a: -(CH <sub>2</sub> ) <sub>5</sub> -	4a: C <sub>6</sub> H <sub>5</sub>	8a	30	92
7a	3b: -(CH <sub>2</sub> ) <sub>2</sub> -O-(CH <sub>2</sub> ) <sub>2</sub> -	4a	8b	35	90
7a	3c: -(CH <sub>2</sub> ) <sub>4</sub> -	4a	8c	40	80
7b: -(CH <sub>2</sub> ) <sub>5</sub> -	3a	4a	8d	43	85
7b	3a	4b: <i>p</i> -CH <sub>3</sub> -C <sub>6</sub> H <sub>4</sub>	8e	50	80
7b	3b	4a	8f	40	90
7b	3b	4b	8g	50	91
7b	3c	4a	8h	38	90
7b	3b	4c: <i>p</i> -F-C <sub>6</sub> H <sub>4</sub>	8i	30	84

<sup>a</sup>Reaction conditions: ketones (1.5 mmol), amines (1 mmol), alkynes (1.5 mmol), h-Fe<sub>2</sub>O<sub>3</sub>@SiO<sub>2</sub>/g-C<sub>3</sub>N<sub>4</sub>/Ag (20 mg) in water at 80 W and room temperature.

<sup>b</sup>Isolated yield.

**SCHEME 3** Plausible mechanism of the A<sup>3</sup>-coupling reaction by h-Fe<sub>2</sub>O<sub>3</sub>@SiO<sub>2</sub>/g-C<sub>3</sub>N<sub>4</sub>/Ag**SCHEME 4** The model reaction of 1H-Tetrazole

the structure of the catalyst was almost preserved in the course of the reaction.

To further investigate the nature of the recycled catalyst and verify whether the structure of the catalyst would

be preserved upon recycling, the XRD pattern of the recycled catalyst was recorded and compared with that of the fresh one, Figure 13. The comparison of two XRD patterns showed their similarity, indicating that the magnetic nanocatalyst would not be destructed upon recycling.

### 3.4 | Comparison of catalytic activity of h-Fe<sub>2</sub>O<sub>3</sub>@SiO<sub>2</sub>/g-C<sub>3</sub>N<sub>4</sub>/Ag with other recently reported

Finally, to study the merits of h-Fe<sub>2</sub>O<sub>3</sub>@SiO<sub>2</sub>/g-C<sub>3</sub>N<sub>4</sub>/Ag, the catalytic activities of this catalyst for promoting two model reactions for the synthesis of propargylamines and 1H-tetrazole were compared with those of some previously reported catalysts, Table 5. As shown, in the case of synthesis of model propargylamine various catalysts under different reaction conditions have been reported (Table 5, entries 1–14). Comparing the magnetic catalysts, entries 1–5, It can be clearly concluded that the catalytic activity of Ag(0) doped organic–inorganic hybrids of h-Fe<sub>2</sub>O<sub>3</sub> is superior to bare Fe<sub>2</sub>O<sub>3</sub>. Moreover, the catalytic activities of the magnetic Ag(0) doped hybrids are comparative, indicating the efficiency of these systems as catalysts. Other catalysts reported for the synthesis of propargylamines led to lower yields. Additionally, compared to h-Fe<sub>2</sub>O<sub>3</sub>@SiO<sub>2</sub>/g-C<sub>3</sub>N<sub>4</sub>/Ag, the reaction times

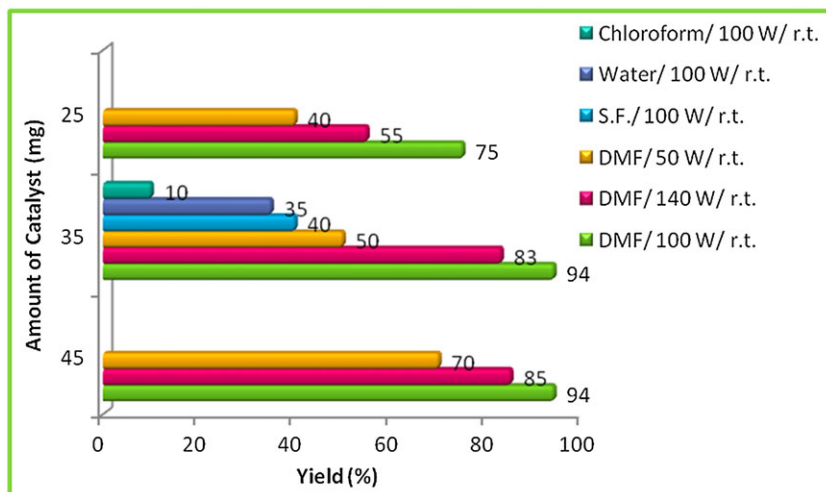


**FIGURE 10** Effects of loading of catalyst, duration of reaction and solvent for the synthesis of 1H-Tetrazole

**TABLE 4** Synthesis of 5-substituted-1H-tetrazole from derivatives of aryl cyanide and sodium azide catalyzed by h-Fe<sub>2</sub>O<sub>3</sub>@SiO<sub>2</sub>/g-C<sub>3</sub>N<sub>4</sub>/Ag<sup>a[50]</sup>

$$\text{R}-\text{C}\equiv\text{N} + \text{NaN}_3 \xrightarrow[\text{DMF/100 W/ r.t.}]{\text{h-Fe}_2\text{O}_3@\text{SiO}_2/\text{g-C}_3\text{N}_4/\text{Ag (30 mg)}} \text{Product= 9a-9o}$$

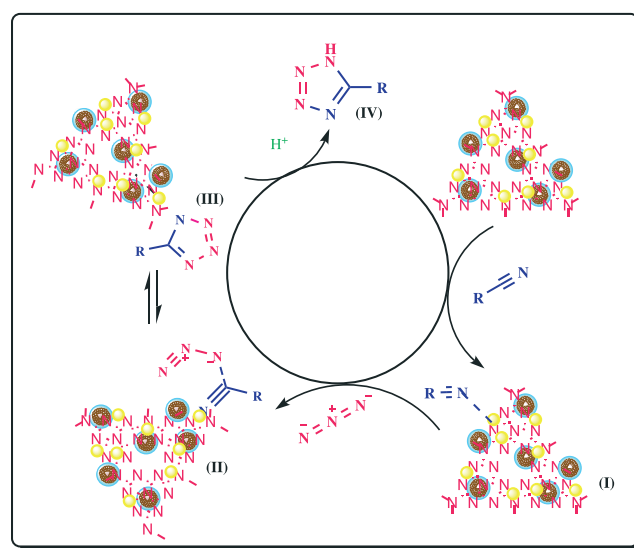
R = Aryl

R	Product	Time (h:min)	Yield (%) <sup>b</sup>
C <sub>6</sub> H <sub>5</sub>	<b>9a</b>	1:30	94
<i>p</i> -O <sub>2</sub> N-C <sub>6</sub> H <sub>4</sub>	<b>9b</b>	1:15	88
<i>p</i> -CH <sub>3</sub> -C <sub>6</sub> H <sub>4</sub>	<b>9c</b>	2	85
<i>p</i> -OCH <sub>3</sub> -C <sub>6</sub> H <sub>4</sub>	<b>9d</b>	2:40	80
β-Naphtol	<b>9e</b>	1:15	80
Α-Naphtol	<b>9f</b>	2	75
<i>m</i> -Cl-C <sub>6</sub> H <sub>4</sub>	<b>9g</b>	1:30	85
<i>p</i> -Cl-C <sub>6</sub> H <sub>4</sub>	<b>9h</b>	1:45	88
<i>p</i> -Br-C <sub>6</sub> H <sub>4</sub>	<b>9i</b>	1:20	90
<i>p</i> -OH-C <sub>6</sub> H <sub>4</sub>	<b>9j</b>	3	85
<i>p</i> -CN-C <sub>6</sub> H <sub>4</sub>	<b>9k</b>	1	88
2-Pyridine	<b>9l</b>	1:10	85
4-Pyridine	<b>9m</b>	1	90
CH <sub>2</sub> -C <sub>6</sub> H <sub>5</sub>	<b>9n</b>	3:30	75
<i>o</i> -NH <sub>2</sub> - <i>m</i> -NO <sub>2</sub> -C <sub>6</sub> H <sub>4</sub>	<b>9o</b>	2:45	80

<sup>a</sup>Reaction condition: nitriles (1.0 mmol), Sodium azide (1.5 mmol), h-Fe<sub>2</sub>O<sub>3</sub>@SiO<sub>2</sub>/g-C<sub>3</sub>N<sub>4</sub>/Ag (30 mg), DMF (5 ml), at 100 W and room temperature.

<sup>b</sup>Yields are after work-up.

for most of those protocols were very long. The comparison of the catalytic activities of h-Fe<sub>2</sub>O<sub>3</sub>@SiO<sub>2</sub>/g-C<sub>3</sub>N<sub>4</sub>/Ag for promoting the synthesis of the model 1H-tetrazole



**SCHEME 5** Plausible mechanism for the synthesis of 5-Substituted 1H-Tetrazoles by h-Fe<sub>2</sub>O<sub>3</sub>@SiO<sub>2</sub>/g-C<sub>3</sub>N<sub>4</sub>/Ag

with some reported catalysts, Table 5, entries 15–23, showed that h-Fe<sub>2</sub>O<sub>3</sub>@SiO<sub>2</sub>/g-C<sub>3</sub>N<sub>4</sub>/Ag could promote the reaction in shorter reaction times to afford the desired product in higher or comparative yield. All these results established that h-Fe<sub>2</sub>O<sub>3</sub>@SiO<sub>2</sub>/g-C<sub>3</sub>N<sub>4</sub>/Ag could be considered as an efficient catalyst for catalyzing organic transformations.

### 3.5 | Spectral data of some selected compound

**1-(1,3-diphenylprop-2-ynyl)piperidine (Table 2, 5a):** Pale yellow oily liquid; <sup>1</sup>H NMR (400 MHz, CDCl<sub>3</sub>, ppm) δ 1.45–1.49 (m, 2H), 1.58–1.65 (m, 4H), 2.59 (t, 4H), 4.81 (s, 1H), 7.31–7.40 (m, 6H), 7.53–7.55 (m, 2H), 7.65–67 (d, *J* = 7.6 Hz, 2H).

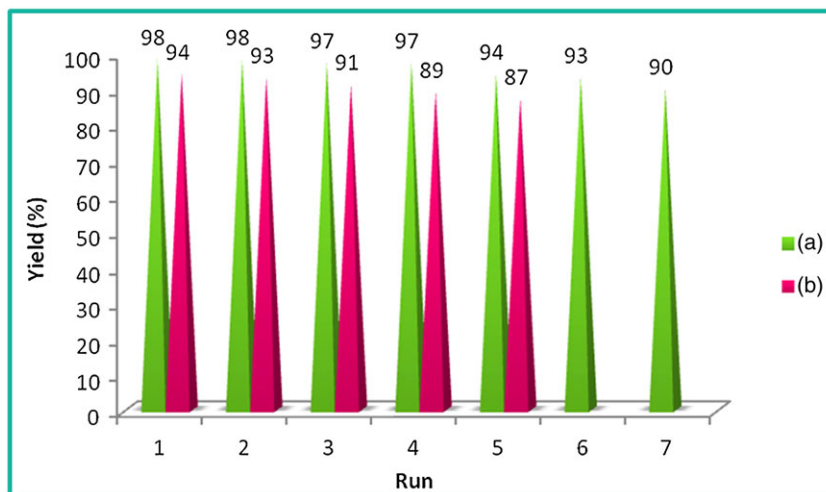


**FIGURE 11** Reusability of the  $\text{h-Fe}_2\text{O}_3@/\text{SiO}_2/\text{g-C}_3\text{N}_4/\text{Ag}$  catalyst for the synthesis of propargylamine (a) and 1H-tetrazole (b)

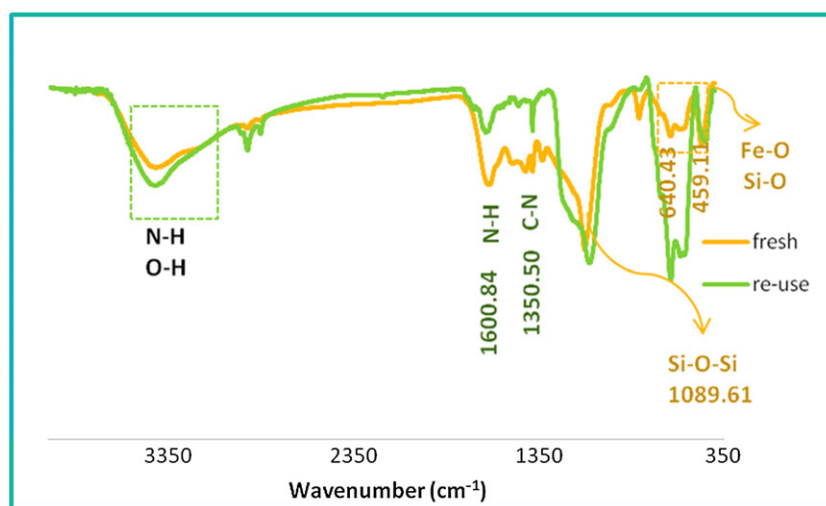


**FIGURE 12** The comparison of FTIR analysis for fresh  $\text{h-Fe}_2\text{O}_3@/\text{SiO}_2/\text{g-C}_3\text{N}_4/\text{Ag}$  and after seven runs

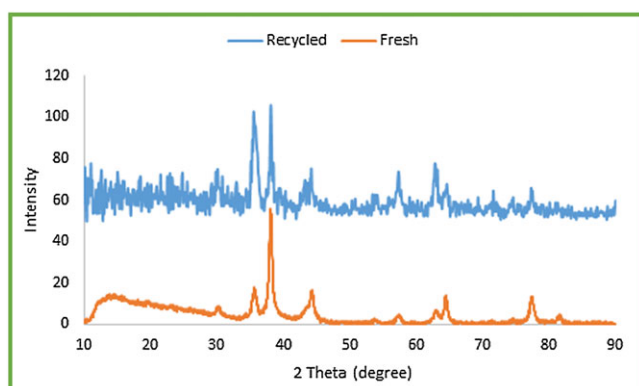


**FIGURE 13** The comparison of the XRD patterns of fresh and recycled catalysts

**1-(3-phenyl-1-(thiophen-2-yl)prop-2-ynyl)piperidine (Table 2, 5g):** Yellow solid; mp 50–51 °C (Lit.<sup>[50]</sup> 52–53 °C);  $^1\text{H}$  NMR (400 MHz,  $\text{CDCl}_3$ , ppm)  $\delta$  1.48–1.52 (m, 2H), 1.63–1.70 (m, 4H), 2.62–2.71 (m, 4H), 5.03 (s, 1H),

7.00 (dd,  $J^1 = J^2 = 3.6$  Hz, 1H), 7.25–7.30 (m, 1H), 7.31 (d,  $J = 4.4$  Hz, 2H), 7.36–7.38 (m, 3H), 7.54–7.57 (m, 2H);  $^{13}\text{C}$  NMR (100 MHz,  $\text{CDCl}_3$ , ppm)  $\delta$  24.4, 26.1, 50.6, 58.2, 85.3, 86.9, 123, 125.3, 125.8, 126.2, 128.2, 128.3, 131.8, 144.

**1-(3-phenyl-1-(4-(3-phenyl-1-(piperidin-1-yl)prop-2-ynyl)phenyl)prop-2-ynyl)piperidine (Table 2, 5h):** White solid; mp 157–159 °C (Lit.<sup>[50]</sup> 158–160 °C);  $^1\text{H}$  NMR (400 MHz,  $\text{CDCl}_3$ , ppm)  $\delta$  1.47 (m, 2H), 1.59–1.63 (m, 4H), 2.59 (m, 4H), 4.81 (s, 1H), 7.33–7.35 (m, 3H), 7.52–7.55 (m, 2H), 7.63 (s, 2H).

**1-(1-(naphthalen-3-yl)-3-phenylprop-2-ynyl)piperidine (Table 2, 5i):** Yellow oil;  $^1\text{H}$  NMR (400 MHz,  $\text{CDCl}_3$ , ppm)  $\delta$  1.47–1.51 (m, 2H), 1.60–1.67 (m, 4H), 2.64 (t, 4H), 4.97 (s, 1H), 7.36–7.40 (m, 3H), 7.48–7.52 (m, 2H), 7.58–7.61 (m, 2H), 7.79 (dd,  $J^1 = J^2 = 8.4$  Hz, 1H), 7.85–7.91 (m, 3H), 8.11 (s, 1H);  $^{13}\text{C}$  NMR (100 MHz,  $\text{CDCl}_3$ , ppm)  $\delta$  24.4, 26.2, 50.8, 62.5, 86, 88.1, 123.3, 125.8, 125.9, 126.7, 127.2, 127.5, 127.7, 128.1, 128.12, 131.8, 132.9, 133.1, 136.3.

**TABLE 5** Comparison of h-Fe<sub>2</sub>O<sub>3</sub>@SiO<sub>2</sub>/g-C<sub>3</sub>N<sub>4</sub>/Ag with other recently reported metal catalysts for the synthesis of propargylamine<sup>a</sup> (Entry 1–14) and 1H-tetrazole<sup>b</sup> (Entry 15–23)

Entry	Catalyst	Reaction conditions	Time (min)	Catalyst amount	Yield (%)	[Ref]
1	h-Fe <sub>2</sub> O <sub>3</sub> @SiO <sub>2</sub> /g-C <sub>3</sub> N <sub>4</sub> /Ag	H <sub>2</sub> O / r.t./U.S	12	20 mg	98	This work
2	h-Fe <sub>2</sub> O <sub>3</sub> @SiO <sub>2</sub> -IL/Ag	H <sub>2</sub> O/ r.t./ U.S	12	25 mg	96	[35]
3	h-Fe <sub>2</sub> O <sub>3</sub> @DA/Ag	S.F./ 90 °C	60	10 mg	96	[50]
4	h-Fe <sub>2</sub> O <sub>3</sub> @SiO <sub>2</sub> -CD/Ag	H <sub>2</sub> O/ r.t./ U.S	8	20 mg	97	[51]
5	h-Fe <sub>2</sub> O <sub>3</sub>	H <sub>2</sub> O/ r.t./ U.S	12	25 mg	75	This work
6	ZnO nano particles	Stirrer/ 90 °C	120	10 mol%	89	[23]
7	Immobilized Silver on Surface-modified ZnO NPs	Reflux/ H <sub>2</sub> O	240	10 mol%	89	[60]
8	Ag-CIN-1 <sup>c</sup>	H <sub>2</sub> O/ 40 °C	720	5 mg	65	[61]
9	Ag <sup>I</sup> -Pc-L <sup>d</sup>	Toluene/MW/ 150 °C	20	3 mol%	59	[62]
10	CuNPs/TiO <sub>2</sub>	Neat/ 70 °C	420	0.5 mol%	91	[19]
11	ZnS	Reflux/ CH <sub>3</sub> CN	270	10 mol%	89	[63]
12	sulfonate-based Cu(I) metal–organic frameworks	Reflux/EtOH, 90 °C	1440	20 mg	87	[33]
13	CuI catalysts supported on protonated trititanate nanotubes	Solvent-free, 70 °C	90	20 mg	95	[64]
14	Cu <sub>2</sub> O/nano-CuFe <sub>2</sub> O <sub>4</sub>	Solvent-free, 90 °C	40	10 mg	93	[31]
15	copper nanoparticles supported on starch micro particles	THF, 60 °C	1200	0.3 mol%	95	[34]
16	Cu(II) Schiff base complex immobilized on graphene oxide	Water, reflux, N <sub>2</sub>	900	20 mg	83	[32]
17	Cu(II) immobilized on Fe <sub>3</sub> O <sub>4</sub> @SiO <sub>2</sub> @L-Arginine	PEG, 120 °C	360	30 mg	97	[54]
18	CoY Zeolite	DMF, 120 °C	840	29 mg	90	[37]
19	CAES <sup>e</sup>	DMSO, 120 °C	60	1 mol%	95	[41]
20	(NH <sub>4</sub> ) <sub>2</sub> Ce(NO <sub>3</sub> ) <sub>6</sub>	DMF, 110 °C	360	10 mmol%	97	[59]
21	MCMBSA <sup>f</sup>	DMF, 100 °C	480	5 mg	85	[43]
22	h-Fe <sub>2</sub> O <sub>3</sub> @DA/Ag	DMF, 110 °C	420	30 mg	94	[50]
23	h-Fe <sub>2</sub> O <sub>3</sub> @SiO <sub>2</sub> /g-C <sub>3</sub> N <sub>4</sub> /Ag	DMF, r.t./ U.S	90	30 mg	94	This work

<sup>a</sup>Reaction conditions: morpholine (1 mmol), benzaldehyde (1 mmol), phenylacetylene (1.1 mmol) in the presence of different conditions.

<sup>b</sup>Reaction condition: benzonitrile (1 mmol), Sodium azide (1.5 mmol) in the presence of different conditions.

<sup>c</sup>Ag-grafted covalent imine network material.

<sup>d</sup>Ag(I)(Pyridine-Containing Ligand) Complexes.

<sup>e</sup>Cu(II) immobilized on aminated pichlorohydrin activated silica.

<sup>f</sup>benzylated MCM-41 sulfonic acid.

#### **N,N-diethyl-1,3-diphenylprop-2-yn-1-amine**

**(Table 2, 5r):** Pale yellow oily liquid; <sup>1</sup>H NMR (400 MHz, CDCl<sub>3</sub>, ppm) δ 1.04 (m, 6H), 2.36–2.62 (m, 4H), 5.19 (s, 1H), 7.15–7.27 (m, 4H), 7.29–7.38 (m, 3H), 7.39–7.41 (m, 2H).

#### **1-(1-cyclohexyl-3-phenylprop-2-ynyl)pyrrolidine**

**(Table 2, 6d):** Colorless liquid; <sup>1</sup>H NMR (400 MHz, CDCl<sub>3</sub>, ppm) δ 1.05–1.36 (m, 5H), 1.56–1.63 (m, 2H), 1.75–1.79 (m, 6H), 1.82–2.10 (m, 4H), 2.5–2.98 (m, 4H), 3.36–3.38 (d, *J* = 7.6 Hz, 1H), 7.14–7.33 (m, 3H), 7.50–7.63 (m, 2H). <sup>13</sup>C NMR (100 MHz, CDCl<sub>3</sub>, ppm) δ 24.9, 26.9, 27.1, 28.3, 32.7, 33, 42.9, 51.1, 61.1, 86.1, 88.9, 125.9, 128.9, 129.8, 132.6.

#### **4-(1-phenylhex-1-yn-3-yl)morpholine (Table 2,**

**6 h):** Yellow oil; <sup>1</sup>H NMR (400 MHz, DMSO-*d*<sub>6</sub>, ppm) δ 0.97 (m, 3H), 1.45–1.75 (m, 4H), 2.67–2.70 (m, 2H), 2.79–2.83 (m, 2H), 3.82–4.13 (m, 1H), 4.15–4.17 (m, 4H), 7.46–7.50 (m, 3H), 7.62–7.64 (m, 2H).

#### **4-(1-(2-phenylethynyl)cyclohexyl)morpholine**

**(Table 3, 8f):** Pale yellow oily liquid; <sup>1</sup>H NMR (400 MHz, CDCl<sub>3</sub>, ppm) δ 1.28–1.30 (m, 1H), 1.52 (m, 2H), 1.63–1.67 (m, 3H), 1.73 (br.s, 2H), 2.03–2.05 (m, 2H), 2.74 (br.s, 4H), 3.78 (br.s, 4H), 7.27 (m, 3H), 7.44–7.45 (m, 2H), <sup>13</sup>C NMR (100 MHz, CDCl<sub>3</sub>, ppm) δ 22.7, 25.7, 35.4, 46.6, 58.8, 67.4, 86.4, 89.8, 123.4, 127.7, 128.1, 131.7.

**4-(1-((4-fluorophenyl)ethynyl)cyclohexyl)**

**morpholine (Table 3, 8i):** Yellow oil;  $^1\text{H}$  NMR (400 MHz, DMSO- $d_6$ , ppm)  $\delta$  1.26–1.34 (m, 1H), 1.57–1.62 (m, 2H), 1.69–1.78 (m, 3H), 1.80–1.86 (m, 2H), 2.00–2.02 (m, 2H), 2.78 (s, 4H), 3.70 (br.t,  $J = 4.2$  Hz, 4H), 6.97–7.00 (t,  $J = 8.6$  Hz, 2H), 7.32–7.40 (m, 2H);

**5-Phenyl-1H-tetrazole (Table 4, 9a):** White solid; mp 213–215 °C (Lit.<sup>[50]</sup> 214–215 °C);  $^1\text{H}$  NMR (400 MHz, DMSO- $d_6$ , ppm)  $\delta$  7.68 (s, 3H, Ph), 7.92 (s, 2H, Ph);  $^{13}\text{C}$  NMR (100 MHz, DMSO- $d_6$ , ppm)  $\delta$  126.6, 128.6, 130.3, 134.6, 155.

**5-(4-Nitrophenyl)-1H-tetrazole (Table 3, 9b):** Yellow solid; mp 218–219 °C (Lit.<sup>[50]</sup> 220–222 °C);  $^1\text{H}$  NMR (400 MHz, DMSO- $d_6$ , ppm)  $\delta$  8.30 (d, 2H,  $J = 8.4$ , Ph), 8.39 (d, 2H,  $J = 8.8$ , Ar-H);  $^{13}\text{C}$  NMR (100 MHz, DMSO- $d_6$ , ppm)  $\delta$  127.6, 129.1, 131, 149.5.

**5-(4-Methylphenyl)-1H-tetrazole (Table 3, 9c):** White solid; mp 249–251 °C (Lit.<sup>[50]</sup> 247–249 °C);  $^1\text{H}$  NMR (250 MHz, DMSO- $d_6$ , ppm)  $\delta$  2.35 (s, 3H, CH<sub>3</sub>), 7.37 (d, 2H,  $J = 7.6$  Hz, Ph), 7.90 (d, 2H,  $J = 7.5$  Hz, Ph).

**5-(3-Chlorophenyl)-1H-tetrazole (Table 3, 9 g):** White solid; mp 138–140 °C (Lit.<sup>[50]</sup> 137–139 °C);  $^1\text{H}$  NMR (250 MHz, DMSO- $d_6$ , ppm)  $\delta$  7.55 (m, 2H, Ph), 7.96 (d, 1H,  $J = 7.6$ , Ph), 7.99 (s, 1H);  $^{13}\text{C}$  NMR (62.9 MHz, DMSO- $d_6$ , ppm)  $\delta$  125.4, 126.2, 126.4, 130.7, 131.1, 133.9, 154.6.

**5-(4-Chlorophenyl)-1H-tetrazole (Table 3, 9 h):** White solid; mp 251–253 °C (Lit.<sup>[50]</sup> 251–252 °C);  $^1\text{H}$  NMR (400 MHz, DMSO- $d_6$ , ppm)  $\delta$  7.61 (d, 2H,  $J = 8.4$ , Ph), 8.09 (d, 2H,  $J = 8.8$ , Ph).

**5-(4-Hydroxyphenyl)-1H-tetrazole (Table 3, 9j):** White solid; mp 235 °C (Lit.<sup>[50]</sup> 233–234 °C);  $^1\text{H}$  NMR (400 MHz, DMSO- $d_6$ , ppm)  $\delta$  6.91 (d, 2H,  $J = 8.4$ , Ph), 7.58 (d, 2H,  $J = 8.4$ , Ph), 10.11 (s broad, OH);  $^{13}\text{C}$  NMR (100 MHz, DMSO- $d_6$ , ppm)  $\delta$  116.1, 117.4, 128.8, 153.2, 159.8.

**4-(1H-tetrazol-5-yl)-benzonitrile (Table 3, 9 k):** White solid; mp 257–259 °C (Lit.<sup>[50]</sup> 258–260 °C);  $^1\text{H}$  NMR (250 MHz, DMSO- $d_6$ , ppm)  $\delta$  8.06 (d, 2H,  $J = 7.1$ , Ph), 8.19 (d, 2H,  $J = 8.6$ , Ar-H);  $^{13}\text{C}$  NMR (62.9 MHz, DMSO- $d_6$ , ppm)  $\delta$  113.3, 118.1, 127.6, 128.7, 133.1, 155.2, 162.2.

**2-(1H-tetrazol-5-yl)pyridine (Table 3, 9 l):** White solid; mp 210–213 °C (Lit.<sup>[50]</sup> 211–212 °C);  $^1\text{H}$  NMR (400 MHz, DMSO- $d_6$ , ppm)  $\delta$  7.75 (s, 1H, Ph), 8.07 (s, 1H, Ph), 8.20 (d, 1H,  $J = 8.4$  Ph), 8.63 (s, 1H).

**4-(1H-tetrazol-5-yl)pyridine (Table 3, 9 m):** White solid; mp 256–258 °C (Lit.<sup>[50]</sup> 256–258 °C);  $^1\text{H}$  NMR (250 MHz, DMSO- $d_6$ , ppm)  $\delta$  8.10 (d, 2H,  $J = 6.0$ , Ph), 8.77 (d, 2H,  $J = 6.5$ , Ph);  $^{13}\text{C}$  NMR (62.9 MHz, DMSO- $d_6$ , ppm)  $\delta$  120.9, 121.3, 133.8, 149.9, 165.7.

**4 | CONCLUSION**

For the first time, a novel and simple hydrothermal procedure is disclosed for the incorporation of g-C<sub>3</sub>N<sub>4</sub> to h-Fe<sub>2</sub>O<sub>3</sub>@SiO<sub>2</sub>. Additionally, an efficient catalyst, h-Fe<sub>2</sub>O<sub>3</sub>@SiO<sub>2</sub>/g-C<sub>3</sub>N<sub>4</sub>/Ag, was prepared through extract-assisted reduction of silver precursor and immobilization of Ag(0) nanoparticles on h-Fe<sub>2</sub>O<sub>3</sub>@SiO<sub>2</sub>/g-C<sub>3</sub>N<sub>4</sub>. The hybrid system exhibited excellent catalytic activity for promoting ultrasonic-assisted A<sup>3</sup>, KA<sup>2</sup> coupling reactions and [3 + 2] cycloaddition. Moreover, the catalyst was highly reusable and showed only slight Ag leaching upon five recycling tests. High yields, low reaction times, broad substrate scope and eco-friendly nature were the merits of this developed protocol.

**ACKNOWLEDGMENT**

The authors appreciate partial financial supports from Alzahra University and Iran Polymer and Petrochemical Institute. MMH is also thankful to Iran National Science Foundation for the Individual given grant.

**ORCID**

Samahe Sadjadi  <http://orcid.org/0000-0002-6884-4328>  
Majid M. Heravi  <http://orcid.org/0000-0003-2978-1157>

**REFERENCES**

- [1] Y. Li, J. Zhang, Q. Wang, Y. Jin, D. Huang, Q. Cui, G. Zou, *J. Phys. Chem. B* **2010**, *114*, 9429.
- [2] X. Zhang, X. Xie, H. Wang, J. Zhang, B. Pan, Y. Xie, *J. Am. Chem. Soc.* **2013**, *135*, 18.
- [3] J. Wen, J. Xie, X. Chen, X. Li, *Appl. Surf. Sci.* **2017**, *391*, B, 72.
- [4] G. Mamba, A. K. Mishra, *Appl. Catal. B* **2016**, *198*, 347.
- [5] F. Su, M. Antonietti, X. Wang, *Sci. Technol.* **2012**, *2*, 1005.
- [6] X. J. Ye, Y. J. Cui, X. Q. Qiu, X. C. Wang, *Appl. Catal. B* **2014**, *152–153*, 383.
- [7] X. S. Zhang, J. Y. Hu, H. Jiang, *Chem. Eng. J.* **2014**, *256*, 230.
- [8] D. J. Martin, K. P. Qiu, S. A. Shevlin, A. D. Handoko, X. W. Chen, Z. X. Guo, J. W. Tang, *Angew. Chem. Int. Ed.* **2014**, *53*, 9240.
- [9] W.-J. Ong, L.-L. Tan, Y. H. Ng, S.-T. Yong, S.-P. Chai, *Chem. Rev.* **2016**, *116*, 7159.
- [10] M. N. Nadagouda, R. B. Nasir Baig, R. S. Varma, S. Verma, *ACS Sustainable Chem. Eng.* **2016**, *4*, 1661.
- [11] R. A. Molla, M. A. Iqbal, K. Ghosh, S. M. Islam, *Green Chem.* **2016**, *18*, 4649.
- [12] R. A. Molla, M. A. Iqbal, K. Ghosh, Kamaluddin, S. M. Islam, *Dalton Trans.* **2015**, *44*, 6546.
- [13] xX. Su, A. Vinu, S. S. Aldeyab, L. Zhong, *Catal. Lett.* **2015**, *145*, 1388.
- [14] S. Kumar, A. Baruah, S. Tonda, B. Kumar, V. Shanker, B. Sreedhar, *Nanoscale* **2014**, *6*, 4830.

- [15] Z. Zhu, Z. Lu, D. Wang, X. Tang, Y. Yan, W. Shi, Y. Wang, N. Gao, X. Yao, H. Dong, *Appl. Catal. B* **2016**, *182*, 115.
- [16] R. B. Nasir Baig, R. S. Varma, *Chem. Commun.* **2013**, *49*, 752.
- [17] X. Wang, J. Feng, Y. Bai, Q. Zhang, Y. Yin, *Chem. Rev.* **2016**, *116*, 10983.
- [18] M. Harmata, *Organic Mechanisms: Reactions, Stereochemistry and Synthesis*, Springer, **2010**.
- [19] M. J. Albaladejo, F. Alonso, Y. Moglie, M. Yus, *Eur. J. Org. Chem.* **2012**, *2012*, 3093.
- [20] G. Villaverde, A. Corma, M. Iglesias, F. Sanchez, *ACS Catal.* **2012**, *2*, 399.
- [21] S. V. Katkar, R. V. Jayaram, *RSC Adv.* **2014**, *4*, 47958.
- [22] N. Salam, S. K. Kundu, A. Singha Roy, P. Mondal, S. Roy, A. Bhaumik, S. Manirul Islam, *Catal. Sci. Technol.* **2013**, *3*, 3303.
- [23] K. V. V. Satyanarayana, P. Atchuta Ramaiah, Y. L. N. Murty, M. R. Chandra, S. V. N. Pammi, *Catalysis Commun.* **2012**, *25*, 50.
- [24] L. F. Bobadilla, T. Blasco, J. A. Odriozola, *Phys. Chem. Chem. Phys.* **2013**, *15*, 16927.
- [25] M. Hosseini-Sarvari, F. Moeini, *New J. Chem.* **2014**, *38*, 624.
- [26] B. J. Borah, S. J. Borah, K. L. Saikia, D. K. Dutta, *Catal. Sci. Technol.* **2014**, *4*, 4001.
- [27] T. Zeng, W.-W. Chen, C. M. Cirtiu, A. Moores, G. Song, C.-J. Li, *Green Chem.* **2010**, *12*, 570.
- [28] T.-W. Hui, J.-F. Cui, M.-K. Wong, *RSC Adv.* **2017**, *7*, 14477.
- [29] A. M. Munshi, M. Shi, S. P. Thomas, M. Saunders, M. A. Spackman, K. S. Iyer, N. M. Smith, *Dalton Trans.* **2017**, *46*, 5133.
- [30] M. Mirabedini, E. Motamedi, M. Z. Kassaei, *Chin. Chem. Lett.* **2015**, *26*, 1085.
- [31] F. Nemati, A. Elhampour, H. Farrokhi, M. Bagheri Natanzi, *Catal. Commun.* **2015**, *66*, 15.
- [32] S. Kumari, A. Shekhar, D. D. Pathak, *RSC Adv.* **2016**, *6*, 15340.
- [33] P. Li, S. Regati, H.-C. Huang, H. D. Arman, B.-L. Chen, J. C.-G. Zhao, *Chin. Chem. Lett.* **2015**, *26*, 6.
- [34] M. Gholinejad, F. Saadati, S. Shaybanizadeh, B. Pullithadathil, *RSC Adv.* **2016**, *6*, 4983.
- [35] S. Sadjadi, M. M. Heravi, M. Malmir, *Appl. Organomet. Chem.* **2017**.
- [36] T. Hashimoto, K. Maruoka, *Chem. Rev.* **2015**, *115*, 5366.
- [37] V. Rama, K. Kanagaraj, K. Pitchumani, *J. Org. Chem.* **2011**, *76*, 9090.
- [38] M. Tajbakhsh, H. Alinezhad, M. Nasrollahzadeh, T. A. Kamali, *Monatsh. Chem.* **2016**, *147*, 2135.
- [39] A. Kumar, S. Kumar, Y. Khajuria, S. K. Awasthi, *RSC Adv.* **2016**, *6*, 75227.
- [40] A. Ghorbani-Choghamarani, L. Shiri, L. Azadi, *RSC Adv.* **2016**, *6*, 32653.
- [41] N. Razavi, B. Akhlaghinia, *RSC Adv.* **2015**, *5*, 12372.
- [42] S. Kumar, S. Dubey, N. Saxena, S. K. Awasthi, *Tetrahedron Lett.* **2014**, *55*, 6034.
- [43] A. N. Chermahini, M. K. Omran, H. A. Dabbagh, G. Mohammadnezhad, A. Teimouri, *New J. Chem.* **2015**, *39*, 4814.
- [44] S. Sadjadi, M. M. Heravi, M. Daraie, *J. Mol. Liq.* **2017**, *231*, 98.
- [45] M. M. Heravi, E. Hashemi, Y. Shirazi Beheshtiha, S. Ahmadi, T. Hosseinnejad, *J. Mol. Catal. A.* **2014**, *394*, 74.
- [46] S. Sadjadi, M. M. Heravi, M. Daraie, *Res. Chem. Intermed.* **2017**, *43*, 2201.
- [47] S. Sadjadi, M. Eskandari, *Ultrason. Sonochem.* **2013**, *20*, 640.
- [48] S. Sadjadi, M. M. Heravi, *RSC Adv.* **2017**, *7*, 30815.
- [49] S. Sadjadi, M. M. Heravi, *RSC Adv.* **2016**, *6*, 88588.
- [50] A. Elhampour, M. Malmir, E. Kowsari, F. A. Boorboor, F. Nemati, *RSC Adv.* **2016**, *6*, 96623.
- [51] S. Sadjadi, M. Malmir, M. M. Heravi, *RSC Adv.* **2017**, *7*, 36807.
- [52] T. K. H. Ta, M.-T. Trinh, N. V. Long, T. T. M. Nguyen, T. L. T. Nguyen, T. L. Thuoc, B. T. Phan, D. Mott, S. Maenosono, H. Tran-Van, V. H. Le, *Asp.* **2016**, *504*, 1.
- [53] M. Tahir, N. Mahmood, L. Pan, Z.-F. Huang, Z. Lv, J. Zhang, F. K. Butt, S. G. X. Zhang, S. X. Dou, J.-J. Zou, *J. Mater. Chem. A* **2016**, *4*, 12940.
- [54] S. C. Yan, Z. S. Li, Z. G. Zou, *Langmuir* **2009**, *25*, 10397.
- [55] X. Zhang, Y. Niu, Y. Yang, Y. Li, J. Zhao, *New J. Chem.* **2014**, *38*, 4351.
- [56] S. Wang, C. Li, T. Wang, P. Zhang, A. Li, J. Gong, *J. Mater. Chem. A* **2014**, *2*, 2885.
- [57] P. Yuan, P. D. Southon, Z. Liu, M. E. R. Green, J. M. Hook, S. J. Antill, C. J. Kepert, *J. Phys. Chem. C* **2008**, *112*, 15742.
- [58] L. Shi, Y.-Q. Tu, M. Wang, F.-M. Zhang, C.-A. Fan, *Org. Lett.* **2004**, *6*, 1001.
- [59] P. Mani, A. C. Sharma, S. Kumar, S. K. Awasthi, *J. Mol. Catal. A: Chem.* **2014**, *392*, 150.
- [60] F. Movahedia, H. Masrouria, M. Z. Kassaei, *J. Mol. Catal. A.* **2014**, *395*, 52.
- [61] N. Salam, S. K. Kundu, R. A. Molla, P. Mondal, A. Bhaumik, S. M. Islam, *RSC Adv.* **2014**, *4*, 47593.
- [62] M. Trose, M. Dell'Acqua, T. Pedrazzini, V. Pirovano, E. Gallo, E. Rossi, A. Caselli, G. Abbiati, *J. Org. Chem.* **2014**, *79*, 7311.
- [63] N. P. Eagalapati, A. Rajack, Y. L. N. Murthy, *J. Mol. Catal. A.* **2014**, *381*, 126.
- [64] B. R. Prasad Reddy, P. V. Govardhana Reddy, M. V. Shankar, B. N. Reddy, *Asian J. Org. Chem.* **2017**, *6*, 712.

## SUPPORTING INFORMATION

Additional supporting information may be found online in the Supporting Information section at the end of the article.

**How to cite this article:** Sadjadi S, Malmir M, Heravi MM. Preparation of Ag-doped g-C<sub>3</sub>N<sub>4</sub> Nano Sheet Decorated Magnetic  $\gamma$ -Fe<sub>2</sub>O<sub>3</sub>@SiO<sub>2</sub> Core-Shell Hollow Spheres through a Novel Hydrothermal Procedure: Investigation of the Catalytic activity for A<sup>3</sup>, KA<sup>2</sup> Coupling Reactions and [3 + 2] Cycloaddition. *Appl Organometal Chem.* 2018;e4413. <https://doi.org/10.1002/aoc.4413>